The Effect of Triplet States on Non-Photochemical Hole Burning in Cytochrome b_6f and Modified LH2 Complex

Alexandra Trempe

A Thesis
in
The Department
of
Physics

Presented in Partial Fulfillment of the Requirements
for the Degree of Master of Science (Physics) at
Concordia University
Montréal, Québec, Canada

May 2021

CONCORDIA UNIVERSITY
School of Graduate Studies

This is to certify that the thesis prepared

By: **Alexandra Trempe**
Entitled: **The Effect of Triplet States on Non-Photochemical Hole Burning in Cytochrome b_6f and Modified LH2 Complex**

and submitted in partial fulfillment of the requirements for the degree of

Master of Science (Physics)

complies with the regulations of this University and meets the accepted standards with respect to originality and quality.
Signed by the Final Examining Committee:

_____ Examiner
Dr. Laszlo Kalman

_____ Examiner
Dr. Ingo Saltzmann

_____ Supervisor
Dr. Valter Zazubovits

Approved by _____
Alexandre Champange, Chair
Department of Physics

_____ 2021

_____
Pascale Sicotte, Dean
Faculty of Arts and Science

Abstract

The Effect of Triplet States on Non-Photochemical Hole Burning in Cytochrome b6f and Modified LH2 Complex

Alexandra Trempe

Photosynthesis is an extraordinary process responsible for all life on Earth. In better understanding how photosynthetic complexes interact with light, we open up opportunities for advancement in environment research. While at times functionally and structurally similar, it has been shown that oxygenic photosynthetic complexes and anoxygenic photosynthetic complexes in purple bacteria possess differences. For example, oxygenic photosynthetic complexes utilise chlorophyll (Chl) pigment molecules, which absorb in the red and blue regions of visible light. Purple bacteria host bacteriochlorophyll (BChl) pigment molecules, absorbing at wavelengths greater than 800 nm. Important information about the functioning of photosynthetic complexes can be obtained from zero-phonon lines and phonon sidebands of the pigments. These are observed through spectral techniques such as non-photochemical hole burning (NPHB), a type of spectral hole burning. NPHB can be explained using a two-level system, or a double-well potential, which is the simplest manner to describe the protein/pigment energy landscape.

When describing NPHB, the model normally considers both a singlet ground state and a singlet excited state of the pigment. In this thesis, we will explore the limitations of only considering these two electronic state for cytochrome b_6f and a modified purple bacteria light-harvesting complex II (LH2) containing Chls. In particular, we originally set out to observe the illumination-intensity dependence (as seen in cytochrome b_6f) in our modified LH2 to try validating the presence of local heating of the protein by the laser beam causing the NPHB. Unfortunately, we were unable to see local heating. This brought the introduction of a triplet state to explain hole burn depth discrepancies between hole growth kinetic curves and post-burn hole spectra. Our modelling allowed us to see that transient holes caused by triplet states contributed to slower burning of persistent holes with increased intensity, as we had observed. We also examined the case of increased triplet lifetime expected when both complexes were placed in a deuterated solvent. An expected triplet lifetime for both complexes in a deuterated solution is around 2 ms, while we examined triplet lifetimes ranging from 1 ms up to 5 ms. Even with a five-fold increase of the simulated triplet lifetime, it did not match the experimental difference between protonated and deuterated samples. Local heating along with triplet states explain the difference.

Finally, we introduce preliminary data relating to pigment participation in the two-level system. Thermocycling hole recovery results revealed a similar recovery rate for Chls placed in either B800 BChl pockets or somewhere else in modified LH2. However, in both cases, the holes recovered more quickly than in the regular, BChl-containing LH2. Given that the two-level system is usually expected to represent the protein environment, Chls in the same location as BChls were expected to recover similarly. Instead, Chls in different environments recovered similarly, leading to the potential assumption that pigments also contribute to the generalised coordinate of the two-level system.

Acknowledgments

First, my thanks is extended to my family and friends. Thank you to my parents, Linda and Paul, for their continued love and support throughout my studies and always encouraging me to do what I wanted, even when I didn't know what that was. Thank you to my sister, Steph, for giving me a chance to laugh, and to the pets for giving me comfort. Thank you to my grandmother, Rose, for the phone conversations and support through the years. Thank you to my parents-in-law, Simonetta and Mario Orlando, for the food (it was very much appreciated) and never-ending encouragement. Thank you to my brother-in-law, Cecco, for the change of mind I needed. And thanks to the friends (Nour, Stephen, Tom, and everyone else) who reached out during the pandemic to keep in touch and kept me from losing my mind.

Thank you to my husband, Mario Felipe, for supporting me during this journey. It was long, it was tough, but we'll both come out with a master's in the end. Nice!

Thank you to my graduate committee, Dr. Laszlo Kalman and Dr. Ingo Saltzmann, for their questions and comments. This thesis certainly would have been written differently had it not been for your astounding (and sometimes quite simple) observations. Thank you to Dr. Pablo Bianucci for bringing up my name as a candidate to potentially do this master's degree. Thank you to my colleagues (in particular, the other Alex in our group and the lab gang) for your friendship and knowledge, especially during such an isolating time.

Finally, a huge thank you to my supervisor, Dr. Valter Zazubovits. Without your support, encouragement, wisdom, and utmost patience, this degree never would have happened. I hope this thesis can be a testament to how far I've come thanks to you.

Contents

List of Figures

List of Tables

List of Abbreviations

BChl	Bacteriochlorophyll
BRC	Bacterial reaction centre
Chl	Chlorophyll
HGK	Hole growth kinetics
LH1	Light-harvesting complex I
LH2	Light-harvesting complex II
NPHB	Non-photochemical hole burning
PC	Photosynthetic complex
PHB	Photochemical hole burning
PS I	Photosystem I
PS II	Photosystem II
PSB	Phonon sideband
PSBH	Phonon sideband hole
R	Rhodoblastus
SHB	Spectral hole burning
TLS	Two-level system (double-well potential)
ZPH	Zero-phonon hole
ZPL	Zero-phonon line

Chapter 1

Introduction

Development in environmental research is an ongoing hot topic. More specifically, better understanding how photosynthetic complexes interact with light can help us develop better photovoltaic cells and even optimise crop production [Wang et al., 2020]. Photosynthetic complexes themselves can be quite intricate and are categorised into two distinct groups: those belonging to oxygenic photosynthesis and those belonging to anoxygenic photosynthesis. In the case of oxygenic photosynthetic complexes, photosystem II and photosystem I are the photochemical systems responsible for taking in light energy in the red and blue regions of the visible spectrum through the famous chromophore, chlorophyll, and converting it as needed to produce oxygen and glucose. Cytochrome b_6f aids in transferring electrons between the two photosystems. Anoxygenic photosynthetic complexes of purple bacteria are made of a number of light-harvesting complex IIs (LH2) and a single light-harvesting complex I (LH1) surrounding a bacterial reaction centre. LH2 is the initial front for absorbing light with a different photosynthetic pigment, bacteriochlorophyll. There are two types of bacteriochlorophylls in LH2, one which absorbs light at 850 nm and one which absorbs light at 800 nm. The complex is also made up of two different types of polypeptides, α and β subunits, with both pigment-protein and pigment-pigment interactions contributing to the different absorption spectra of the bacteriochlorophylls. Energy is transferred among consecutive complexes until it is centrally directed to LH1's dimer pair of 870-nm-absorbing bacteriochlorophylls. From there, energy is eventually passed to the bacterial reaction centre.

A pigment's spectral data can be better understood through the Franck-Condon principle. The principle states that the probabilities of vibronic (that is, electronic and vibrational) transitions are determined by the overlap of the vibrational wavefunctions, that, in the first approximation, are assumed to be harmonic oscillator wavefunctions. This description, along with linear coupling and the low-temperature approximation, allows us to describe chromophore spectral data through zero-phonon lines and a phonon sideband. Their intensity, width, and position depend on various factors, such as presence of energy or charge transfer, temperature, and electron-phonon coupling strength. However, in a macroscopic sample containing many pigments, individual pigment molecules will experience somewhat different environments and therefore, the individual zero-phonon lines and phonon sidebands disappear under inhomogeneous broadening. Our interest lies in finding these hidden zero-phonon lines. Another complexity which may arise is in describing the pigment in a complicated environment. However, a simple two-level system (also known as a double-well potential) can be used to describe the energy landscape of such a pigment in the protein or another amorphous solid environment. It involves a ground- and excited-state double well configuration where the pigment can move between different wells. This brings us to the spectral technique, spectral hole burning. As the name implies, a hole is "burnt" into the absorption spectra of the pigment. This allows us to identify a zero-phonon hole, the mirror image of a zero-phonon line. The spectral hole burning subcategorical technique, non-photochemical hole burning, allows us to "change" the original environment of the pigment. This environmental change is described as the pigment moving from one well of the excited state to the other through tunnelling, before settling back down into the second well of the ground state. When using this spectral technique, both hole growth kinetics (that is, how the hole burns while it burns) and hole recovery experiments are important in describing the energy landscape and protein dynamics of the pigment.

In this thesis, we will start from the non-photochemical hole burning research of a solvent deuteration effect noted in cytochrome b_6f. That is, we originally noticed an illumination-intensity dependence of hole growth kinetics in cytochrome b_6f which was stronger in deuterated samples. Originally this was hypothesised to be because of local heating. Consequently, we designed a modified LH2 from purple bacteria which replaced

some of their 800-nm-absorbing bacteriochlorophylls with chlorophylls. This was done because a lot of heat is dissipated during energy transfers between 800- and 850-absorbing bacteriochlorophylls in the complex. This meant we could use the bacteriochlorophylls as local heaters and the chlorophylls as local thermometers. So far, we have been unable to illuminate our sample well enough at 800 nm to see a local heating effect. However, we discovered that the chlorophylls in our modified LH2 nonetheless behave in the same manner as in our cytochrome b_6f: 1) the intensity dependence was present and was stronger in deuterated samples, and 2) there was also an observed mismatch between hole growth kinetic depths and actual hole spectra. Thus, we introduced triplet states into our non-photochemical hole burning model to explain our observations. We also briefly examined hole recovery thermocycling experiments in LH2 and how this recovery potentially indicated that the pigment contributes to the generalised coordinate of a two-level system.

In Chapter 2, we will discuss important structural and spectral details of oxygenic and anoxygenic purple bacterial photosynthetic complexes. In Chapter 3, we will go over the finer details of chromophore spectral data and explain spectral hole burning. Chapter 4 will go into depth of the experimental research and results obtained on our modified LH2. Finally, in Chapter 5, we will end with some brief conclusions and avenues for future work.

1.1 Noteworthy Biochemical Terms

The discussion of photosynthesis requires interdisciplinary knowledge of chemistry and biology along with physics, as anyone in the biophysics community can relate to. In order to ensure biochemical jargon is not lost on the reader throughout the thesis, we will briefly outline some important terms which will appear later. The following terminology and concepts have been extracted from [Bruice, 2014] unless noted otherwise.

Polypeptides are polymers of amino acids, which are the basic building blocks of a protein and are made up of carboxylic acid and protonated amino group and linked by amide bonds. The amino acids found in a peptide chain are called *residues*. Proteins can have a wide variety of functions, such as structural proteins which impart strength in a system, or enzymes which catalyze reactions in a cell. A protein is defined by four levels

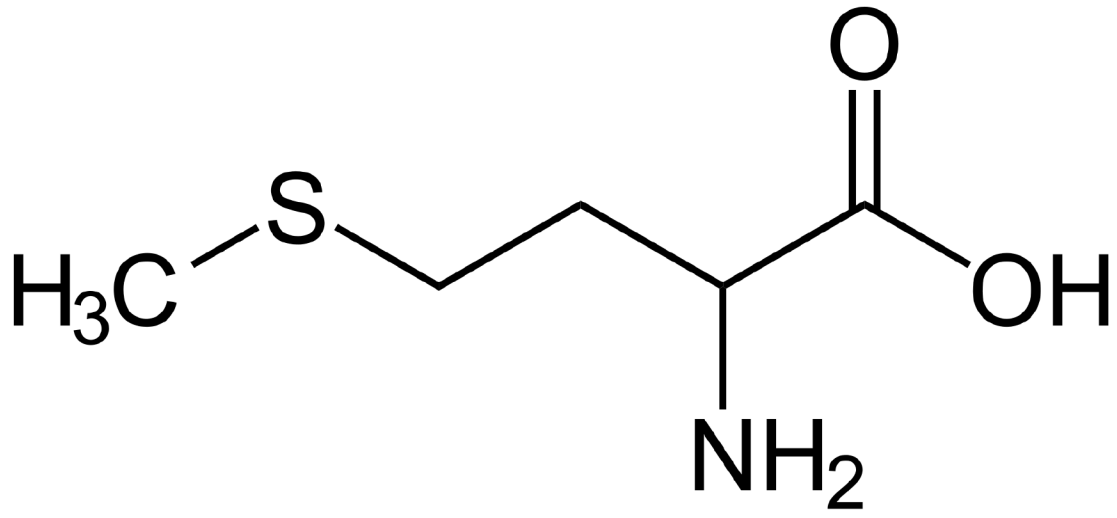

Figure 1.1: Methionine is an example of an essential amino acid.

structurally. The first is the primary structure, which describes the sequence of the amino acids and determines the location of the disulfide bridges, which are the covalent bonds made up of two sulfur atoms and are found between nonadjacent amino acids in proteins. The sequence of the polypeptide is conventionally written from the *N-terminal* amino acid to the *C-terminal* amino acid, where each terminal refers to the free amino group and free carboxyl group respectively.

The secondary structure describes the normal conformation the segments of the protein's backbone chain take on when it folds, such as, for example, the structure of α-helices and β-sheets. The tertiary structure is the three-dimensional structure of the protein responsible for the said protein's intended function. Finally, the quaternary structure is noted when a protein has more than one polypeptide chain, referred to as an *oligomer*. In this case, the different chains are referred to as *subunits*. A single subunit is referred to as a *monomer* and two subunits are called a protein *dimer*. Repeated individual molecules in a larger construct (for example, a microtubule), referred to as a polymer, are also called monomers.

When electrons are forced into a particular part of a compound and either belong to a single atom or shared by two via chemical bonds, they are referred to as localised electrons. When electrons are shared by three or more atoms, they are considered delocalised electrons. Delocalised electrons in a compound lead to stability, where delocalisation energy is a measure of how much more stable a compound is with delocalised electrons compared

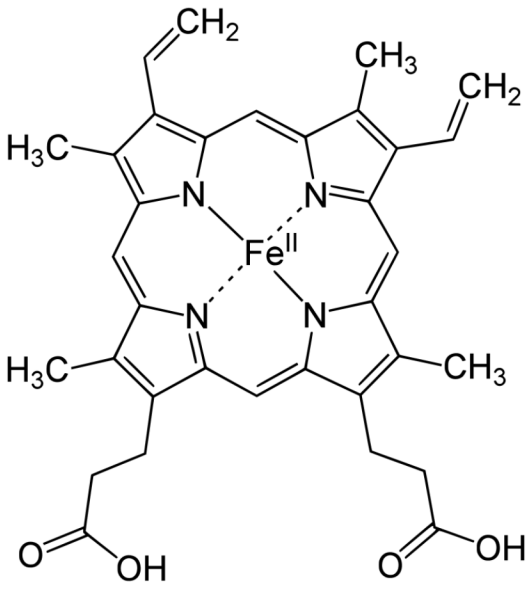

Figure 1.2: An example of a porphyrin ring system, heme-b. Though the iron ion is only shown bound to four nitrogen atoms in this figure, heme is hexacoordinated due to additional axial ligands.

to if it only had localised electrons. Aromatic compounds, such as benzene, have large delocalisation energies, meaning they are stable. In order to be considered aromatic, the compound must be cyclic and planar and have an uninterrupted cloud of an odd-numbered pair of π electrons (that is, there exist three, five, etc. pairs of these two π electrons), consisting of two electrons bound by a π bond such that there is a side-to-side overlap of two parallel, in-phase p orbitals. A *pyrrole*, a heterocyclic compound where the five-membered ring consisting mostly of carbon also contains an N-H group, is aromatic. *Tetrapyrroles* are made up of four pyrroles, or at least four pyrrole-like structures. A *porphyrin* ring system is made up of four pyrroles, like a tetrapyrrole, but in a ring formation. Therefore, a porphyrin is a type of tetrapyrrole. A well-known example of a porphyrin ring system is *heme* (shown in Figure 1.2) found in hemoglobin, myoglobin, and even cytochrome b_6f. It contains a central iron ion which is ligated (where *ligation* is the sharing of lone-pair electrons with a metal ion) by the four nitrogens of a porphyrin. A class of oxidised compounds derived from aromatic compounds called *quinones* are formed when aromaticity is broken in highly reactive aromatic compounds with electron-donating substituents.

A cofactor is an organic molecule or metal ion which can only carry out a chemical

reaction with cooperation with an enzyme [Jones and Fleming, 2010]. When examined biologically, this cofactor is referred to as a coenzyme. A tightly-bound coenzyme is referred to as a *prosthetic group*.

Chromatography refers to a separation technique whereby a mixed solution, referred to as the "eluent", is dissolved in a solvent. In column chromatography, the components in the mixture equilibrate between an absorbent, stationary phase and a moving phase [Jones and Fleming, 2010]. The mobile phase is examined carefully, where each component, the "eluates", from the original mixture is collected individually as it leaves the vessel. There exist different chromatographic techniques, such as *liquid chromatography* and gas chromatography. Both are viable and are used depending on the nature of the substance.

Chapter 2

Photosynthetic Complexes

Photosynthesis is an important process whereby organisms, ranging from plants to certain types of bacteria, convert light energy into chemical energy. The pigment/protein complexes which allow for photosynthesis, known as photosynthetic complexes (PCs), vary depending on whether or not oxygen is a byproduct. In this chapter, we will introduce *photosystem I* (PS I), *photosystem II* (PS II), and *cytochrome* b_6f involved with oxygenic photosynthesis. We will also examine the anoxygenic photosynthetic complexes of purple bacteria, *light harvesting complex I* (LH1), *light harvesting complex II* (LH2), and the *bacterial reaction centre* (BRC).

2.1 Oxygenic Photosynthesis

In plants and particular types of bacteria such as cyanobacteria, the photosynthetic complexes consist of a photosystem II (PS II) and photosystem I (PS I). PS II takes in light energy before transferring it to a special pair of chlorophylls (Chls) at the reaction centre. This chromophore gives way to electron transfer rather than energy transfer. Electrons are then further transferred via quinones and end up reaching cytochrome b_6f. Through the cytochrome b_6f, proton transfers happen along with the electron transfers. Electrons are further transferred to the P700 chlorophyll dimer in PS I. The system is shown in Figure 2.1 and will be detailed in this section.

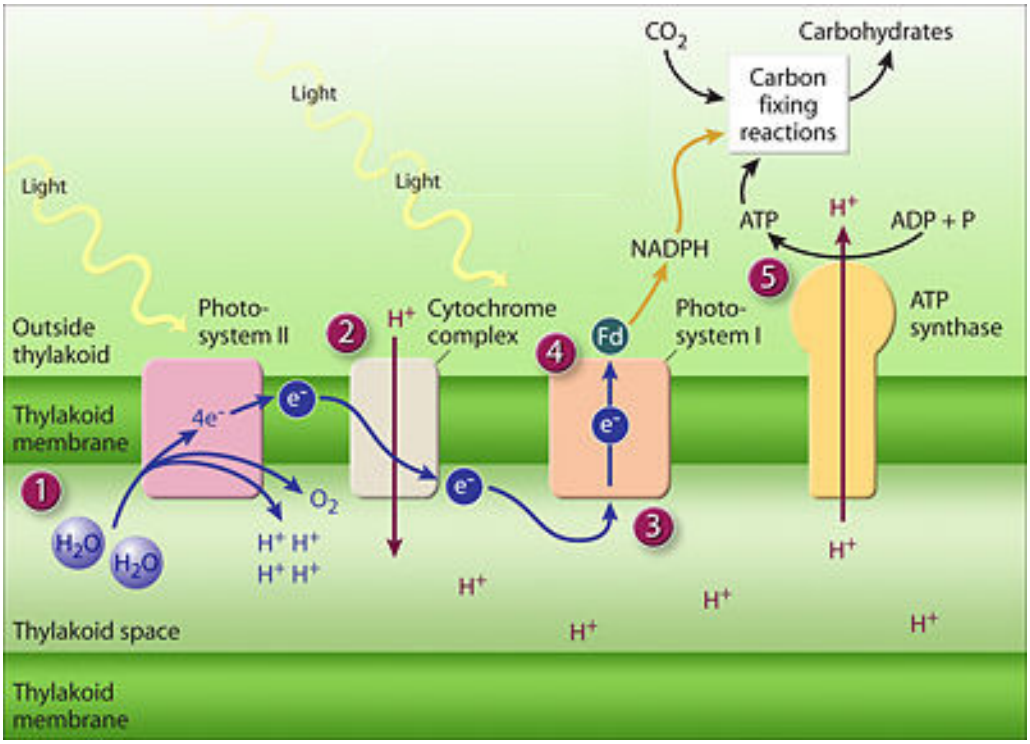

Figure 2.1: The oxygenic photosynthetic system with main components, including photosystem I, cytochrome b_6f, and photosystem II (Image modified from U.S. Department of Energy Genomic Science program as cited in [Sebastien, 2010]).

2.1.1 Chlorophyll (Chl)

Oxygenic photosynthetic complexes contain the pigment molecule chlorophyll (Chl), an essential component of the complex which absorbs light and enables electron transfer [Melkozernov and Blankenship, 2006]. Chls are well-suited for absorbing light in the blue and red spectral region and do not absorb green light, hence why they appear green to the eye [Scheer, 2006]. Structurally, they are a cyclic tetrapyrrole made of partially hydrogenated porphyrins with Mg generally being the central metal in the pigment, though Zn has also been found in some exotic scenarios [Melkozernov and Blankenship, 2006] [Scheer, 2006]. It is generally referred to as chlorin or phytochlorin [Scheer, 2006]. While there exist various types of Chls, the most ubiquitous one is Chl *a*, as shown in Figure 2.2 [Scheer, 2006].

As mentioned above, it is known that Chls absorb light in the red and blue regions of electromagnetic radiation. The absorbance band in the blue region of the visible

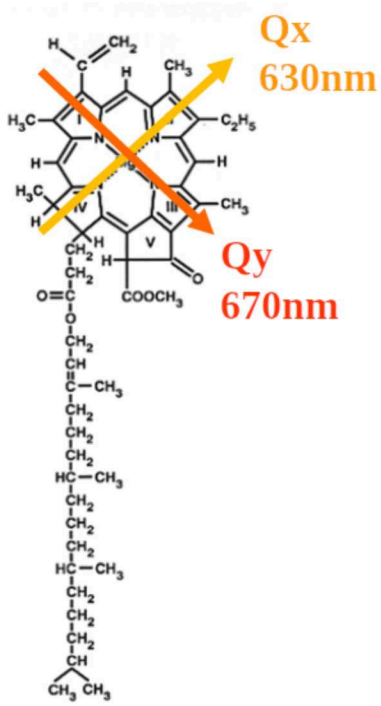

Figure 2.2: Chl *a*, the most common type of Chl pigment. We can see the orientation of the Q_x and Q_y transition dipole moments in the chlorophyll which gives rise to the Q bands. Only the four nitrogens bound to the magnesium ion are shown (Image modified from [Whitmarsh and Govindjee, 1999]).

spectrum, ranging from 400 to 500 nm at room temperature, is referred to as the *Soret band* [de Paula et al., 1995]. The absorption band in the red region, at around 670 nm for Chl *a* at room temperature, is referred to as the *Q band*, made up of a Q_x band and Q_y band [de Paula et al., 1995]. The absorption bands are shifted for different Chl types, such as a red shift of the Soret band and blue shift of the Q band for Chl *b* (see Figure 2.3).

2.1.2 Photosystem II (PS II)

Plants have so-called antenna complexes which are able to harvest light at various wavelengths, ranging from blue light to beyond 700 nm. The first system to harvest this light is called photosystem (PS) II (designated the "second" photosystem simply because it was discovered after PS I, even though it is the first complex involved in photosynthesis from the perspective of electron transfer pathways). The complex is made up of proteins, Chl molecules, and carotenoids. Light will hit the ground-state electrons in the array and

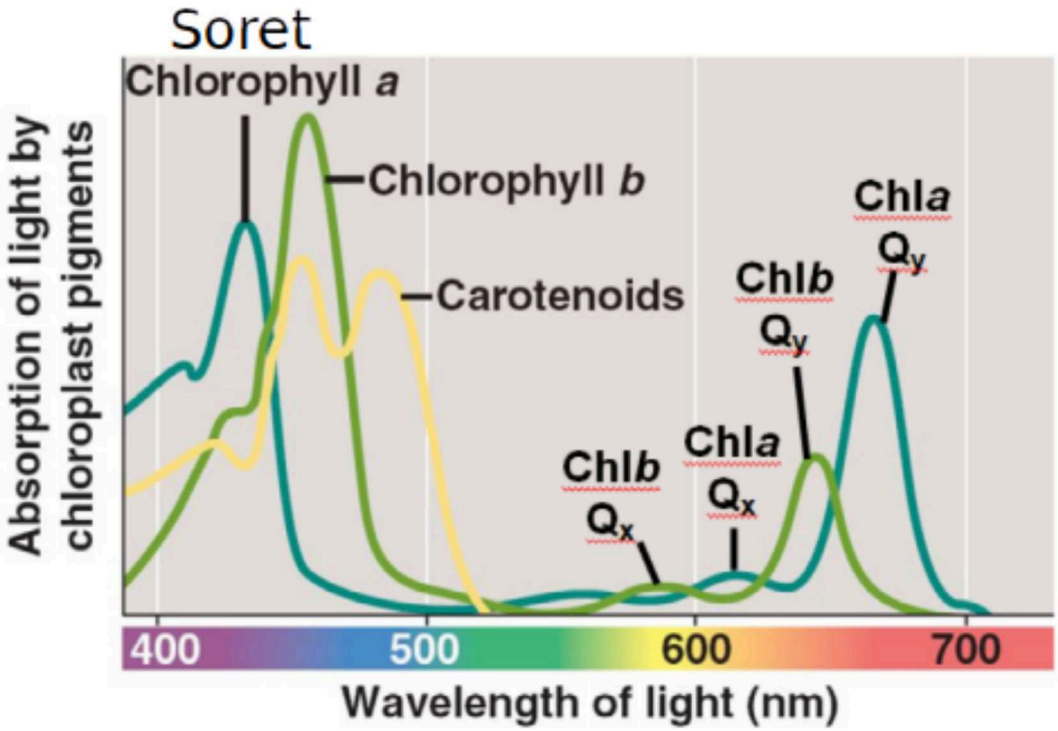

Figure 2.3: The absorption spectra of Chl a (in blue), of Chl b (in green), and carotenoids (in yellow). The absorption band in the blue region is referred to as the Soret band, seen between 400 and 500 nm. The absorption band in the red region is referred to as the Q band, where we see that Q_x has bumps around 600 nm and Q_y has peaks around 650 nm [Chen, 2008].

cause them to become excited. Once the electron decays back down to the ground state, it releases energy which is then transferred to the next chromophore. Electronic excitation energy decreases over the course of this energy exchange. The reaction centre uses a lower energy than originally harvested to perform various functions in the plant cell. This energy exchange is called electronic energy transfer (EET). Thus, electrons are not transferring at this point, only energy.

Energy is transferred across these complexes until it reaches a special pair of Chls, which is considered the core chromophore, residing in the reaction centre. These two Chls form a strongly-coupled dimer whose lowest excitonic state is called P680 (or "pigment 680"). This chromophore gives way to electron transfer rather than energy transfer. In particular, it is transferring an electron through pheophytin (Pheo), which is a Mg-absent chlorophyll

[Klimov, 2003], whereby the electrons accumulate on terminal quinones in PS II. While pigments in the antenna complex are absorbing a photon infrequently enough that the probability of having two excitations occur at the same time is very low, the electrons will add up over time. When the strongly-coupled dimer becomes excited to form the excited pair $P680^*$, it loses the electron in order to form the oxidised $P680^+$ [Shen, 2020]. The $P680^+$ is then reduced by electrons coming from water provided by the oxygen-evolving cluster in the system.

2.1.3 Cytochrome b_6f

Electrons are then transferred via quinones and end up reaching the cytochrome b_6f complex, shown in Figure 2.4. Cytochrome b_6f is a protein complex in the thylakoid membrane. One of its responsibilities is transferring electrons from PS II to PS I, from plastoquinol to plastocyanin [Baniulis et al., 2008]. However, it also significantly contributes to the proton gradient which helps with transmembrane-free energy storage [Hasan et al., 2013]. This in turn allows for the synthesis of ATP [1].

Structurally, cytochrome b_6f is a dimer and each monomer is made up of eight subunits [Baniulis et al., 2008]. The monomeric enzyme also has seven prosthetic groups. Four of these groups are shared with its mitochondriac partner cytochrome bc_1: two b-type hemes, heme b_pm and heme b_n on the p- and n-sides of the cytochrome respectively; a [2Fe-2S] cluster in the Rieske protein [2]; and a c-type heme of cytochromes c_1 and f [Baniulis et al., 2008]. Of more interest given their uniqueness to the enzyme, the other three are Chl *a*, β carotene, and heme c_n [Baniulis et al., 2008]. The role of the Chls in cytochrome b_6f is unknown, as it seems they are not part of the electron transfer chain and their light-harvesting capabilities are pointless, given the lack of an RC in the cytochrome complex [Najafi et al., 2015]. A presumed reason is simply that they are an evolutionary relic of sorts.

[1] ATP, or adenosine triphosphate, is an organic compound which becomes involved in the Calvin cycle (the reactions in the organism which result in the formation of oxygen and glucose formation) of plants to produce glucose.

[2] A Rieske protein is an iron–sulfur protein part of both cytochrome bc_1 and cytochrome b_6f.

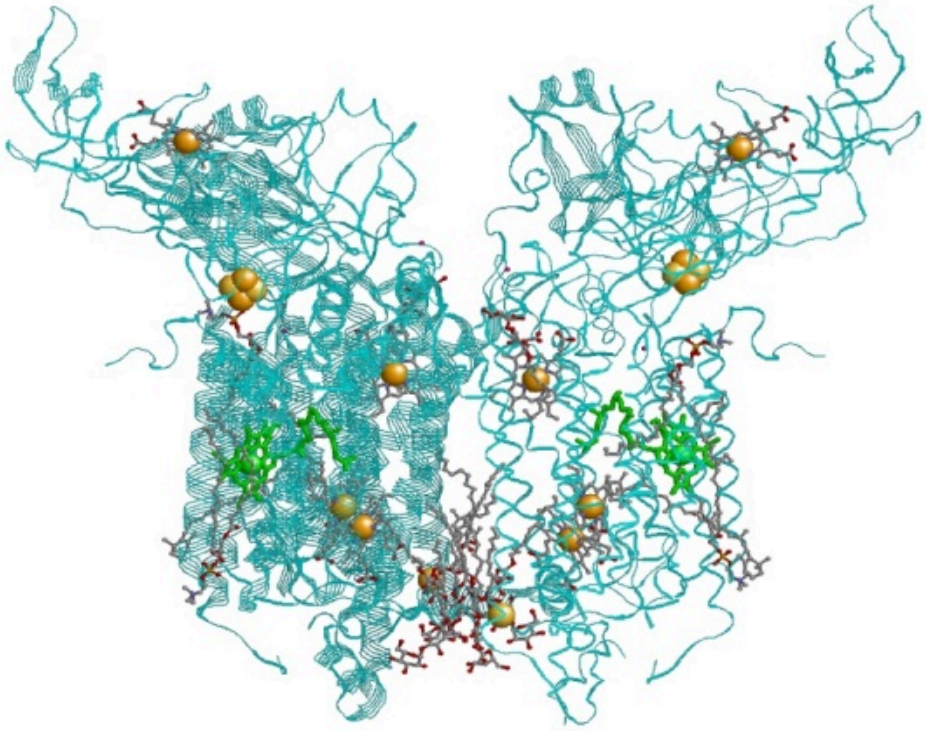

Figure 2.4: The structure of cytochrome b_6f. The iron clusters and iron found in heme proteins are in gold, whereas Chl *a*'s are shown in green.

2.1.4 Photosystem I (PS I)

From cytochrome b_6f, electrons are then transferred to PS I. Larger than PS II [Nelson and Yocum, 2006], it is nonetheless also made up of proteins and Chl molecules. Like PS II, it contains a special pair of Chls at the centre; however, they are P700 Chls rather than P680, meaning light is absorbed at 700 nm. The complex allows the light-induced transfer of electrons from plastoquinol to ferredoxin, where ferredoxin reduces $NADP^+$ into NADPH [Nelson and Yocum, 2006].

2.2 Anoxygenic Photosynthesis in Purple Bacteria

In purple bacteria, their photosynthetic complexes consist of peripheral antenna complexes called light-harvesting complex II (LH2), which then transfer energy to light-harvesting complex I (LH1). LH1 transfers excitation energy to the bacterial reaction centre (BRC) it surrounds [Robert et al., 2003]. See Figure 2.5.

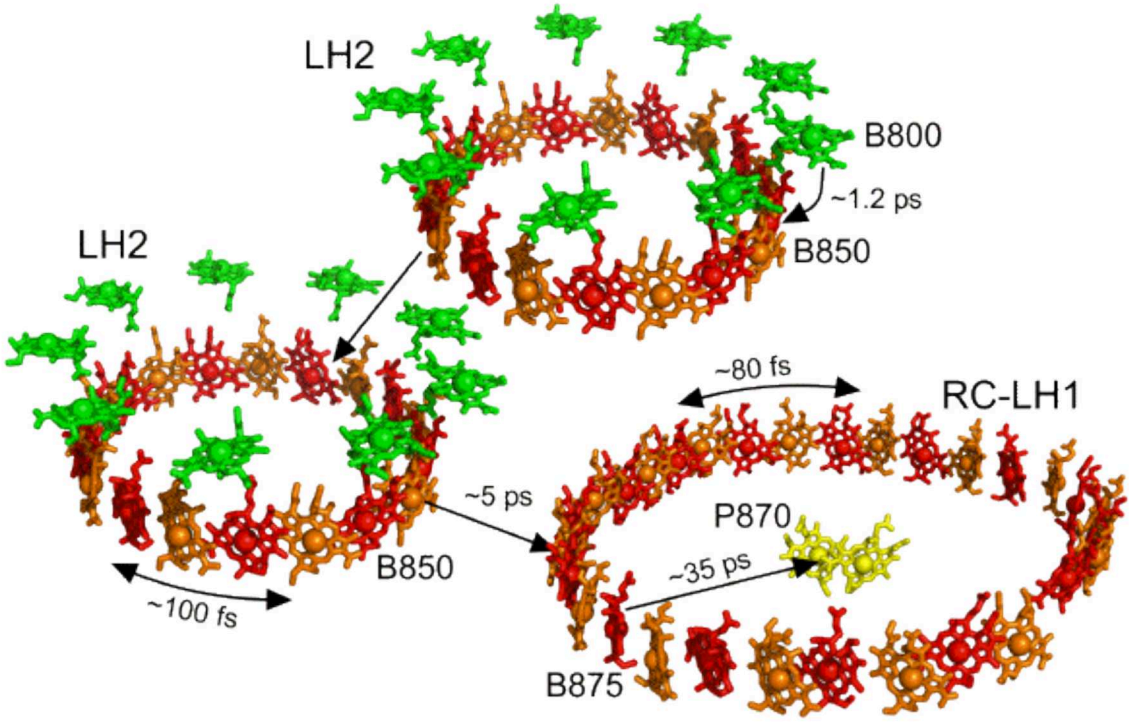

Figure 2.5: The anoxygenic photosynthetic system of purple bacteria with multiple LH2s and single LH1-BRC. Only the special pair of the BRC, P870, is shown [Jones, 2009].

2.2.1 Bacteriochlorophyll (BChl)

While oxygenic photosynthetic complexes contain the well-known chlorophyll (Chl), anoxygenic photosynthetic bacterial complexes contain what are referred to as bacteriochlorophylls (BChls). In particular types of bacteria, such as green sulfur bacteria, certain forms of BChls (such as BChl *c*, *d*, and *e*) present in their complexes are phytochlorins [Scheer, 2006]. However, we will focus our attention on true bacteriochlorins or tetrahydroporphyrins, which are generally the sole type of chlorin found in purple bacteria [Scheer, 2006] [Senge and Smith, 2004]. Rings B and D in these bacteriochlorins are hydrogenated, which leads to an increased gap in the absorption spectrum compared to its chlorin counterpart given a red shift of the Q_y absorption band and a blue shift of the Soret band [Scheer, 2006].

In purple bacteria, the most prevalent type of bacteriochlorin is BChl *a*, shown in Figure 2.6. It is found in their peripheral antenna complexes, as well as in the LH1 and BRC in most anoxygenic photosynthesis bacteria. BChl *a* may also be replaced by BChl *b* in the

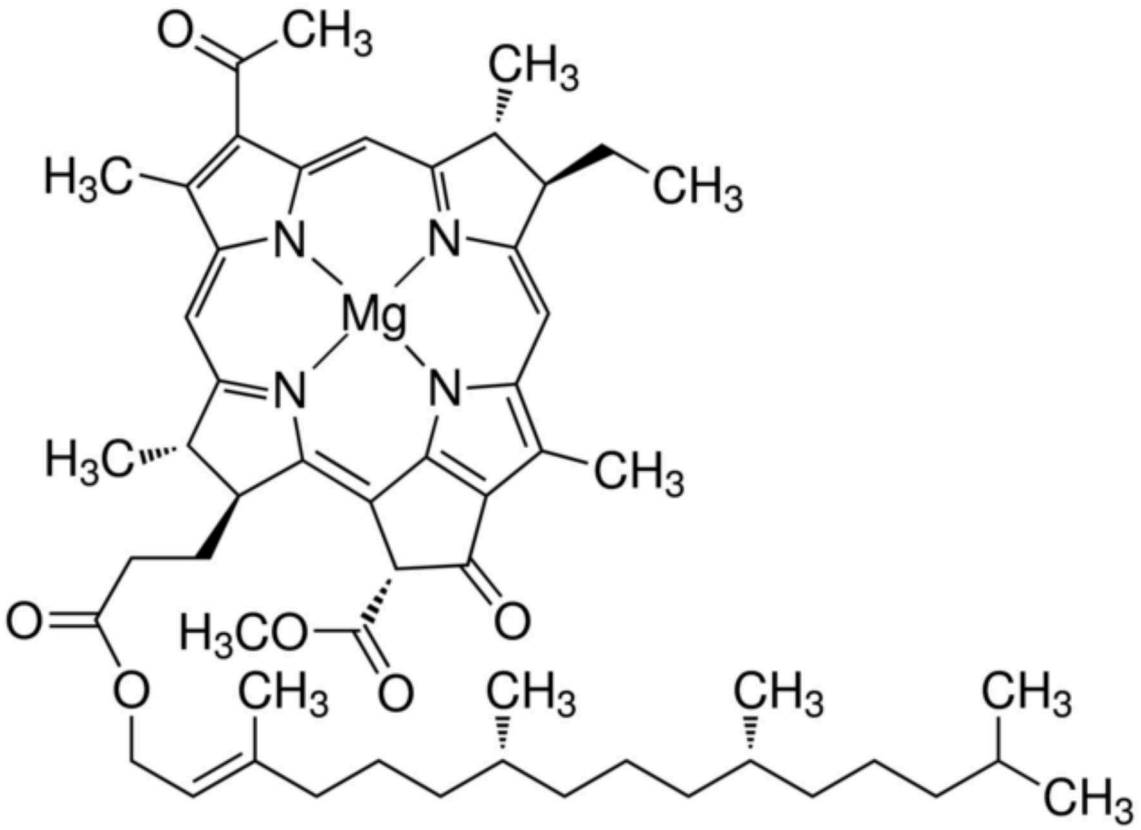

Figure 2.6: An example of a BChl, type BChl *a*. This type of bacterial pigment is the most ubiquitous. In this figure, only the four nitrogens bound to the magnesium ion are shown, but the coordination number is actually six with additional axial ligands [Sigma-Aldrich, 2021].

LH2 complex, such as in Blastochloris (B.) viridis. BChl *b* contains an 8-ethylide group instead of the 8-ethyl group found in BChl *a*. When placed in organic solvents outside of the protein, BChls will absorb at approximately 773 nm [Kühlbrandt, 1995]. However, BChls within the antenna complexes will absorb at different wavelengths due to varying local environments or inter-pigment interactions. This will be further explored in Sections 2.2.3 and 2.2.4.

2.2.2 α and β Subunits

Within each antenna complex in purple bacteria, that is, both LH2 and LH1, there exist two different antenna polypeptides, α and β. The two are structurally and sequentially similar [Brunisholz and Zuber, 1992]. In the α subunit, there are two histidine (His)[3] residues ,

[3]Histidine is an α-amino acid.

whereas in the β subunit, there are three [Alia et al., 2001]. For both α and β, one of the His residues acts as the ligand to the BChl [Brunisholz and Zuber, 1992] [Bullough et al., 2009]. In addition, in the β polypeptide, there is a second His residue present which also acts as a BChl-binding site [Bullough et al., 2009].

The α β polypeptides form two concentric, circular oligomers in the antenna complexes, with the β on the outside and the α on the inside [Berlin et al., 2007].

2.2.3 Light-Harvesting Complex II (LH2)

LH2, as shown in Figure 2.7, is the peripheral antenna complex responsible for taking in light. It is a ring-like structure consisting of BChls, where each of the eight or nine α β subunits contain three BChls and one carotenoid, with the BChls and carotenoid sandwiched between the two α β polypeptides when examined in the membrane plane [Robert et al., 2003] [Young and Beatty, 2003]. For Rhodoblastus (R.) acidophilus, the strain we used in our experiments, there are nine α β subunits. Each α β subunit contains one BChl a which absorbs at 800 nm at room temperature, two BChl a's which absorb at 850 nm at room temperature, and one carotenoid [Robert et al., 2003] [Brunisholz and Zuber, 1992] [Berlin et al., 2007]. When examined in the membrane plane, the 800 nm-absorbing BChls are centred, though closer to the cytoplasm or N-terminal of the subunit, whereas 850 nm-absorbing BChls a are closer to the periplasmic (outer) membrane or C-terminal, noted in Figure 2.7 by the "spaghettini" strands sticking out of the main polypeptide, of the subunit [Brunisholz and Zuber, 1992].

The BChl a's which absorb at 800 nm or at 850 nm are designated as B800 and B850 BChls respectively, where the B stands for "bulk BChl" [Brunisholz and Zuber, 1992]. The reason for their differing absorption is due to their placement and environment. The B800 BChls are closer to the N-terminal. The BChl is held there partially due to a formylated methiodine of the N-terminal of the α polypeptide acting as a ligand to the centre magnesium ion of the BChl [Kühlbrandt, 1995]. For B800 BChl protrusion through the β polypeptide, it is held there due to an intramolecular, buried ionic pair in the polypeptide which forms a strong hydrogen bond with the carbonyl group of the BChl a [Kühlbrandt, 1995]. Given these two factors and the presence of a water molecule, the

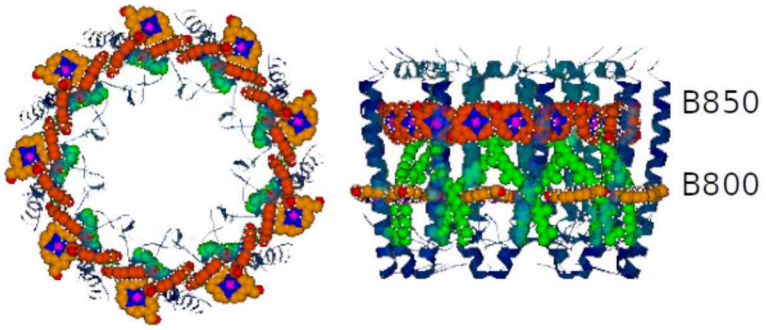

Figure 2.7: Light-harvesting complex II (LH2), with a view from the cytoplasmic plane (perpendicular to the membrane plane) on the left and the membrane plane with cytoplasm side down on the right. B800 BChls are shown in orange and B850 BChls are shown in red and blue.

environment in the middle of these α β polypeptides is polar enough to induce a red shift to around 800 nm for these BChls. The B850 BChls are closer to the periplasm when examined in the membrane plane. The local environment of the BChls causes a red shift from 773 nm in organic solvents to approximtely 800 nm in LH2 as seen for the B800 BChls. Further red-shifting is seen due to the strong coupling between all nearest neighbours in the ring, thus leading to B850 BChls [Kühlbrandt, 1995]. This strong coupling coherently delocalises the excitation of the BChl molecules over a large part of the LH2. This leads to the formation of exciton states, shown in Figure 2.9 [Ritz et al., 2002] [Zazubovich et al., 2002]. The doubly-degenerate, second lowest exciton state contains most of the oscillator strength of the B850 ring, meaning it contributes to light absorption [Zazubovich and Jankowiak, 2015]. The lowest energy level is normally forbidden in idealised (symmetrically and geometrically) conditions, but disorder allows for some oscillator strength [Ritz et al., 2002] [Zazubovich and Jankowiak, 2015].

Due to these two differently absorbing pigments, LH2 can either take in light at 800 nm or 850 nm. Consequently, there are also transitions occurring between B800-B800, B800-B850, and B850-B850 BChls. Of particular note, the B800-B850 transition, which occurs in 1.6 picoseconds (ps) at room temperature, is due to an extended Förster energy transfer [Mukai et al., 1999] [Scholes and Fleming, 2000] and the transition results in heat dissipation [Kühlbrandt, 1995] [Berlin et al., 2007] [Zazubovich and Jankowiak, 2015]. In

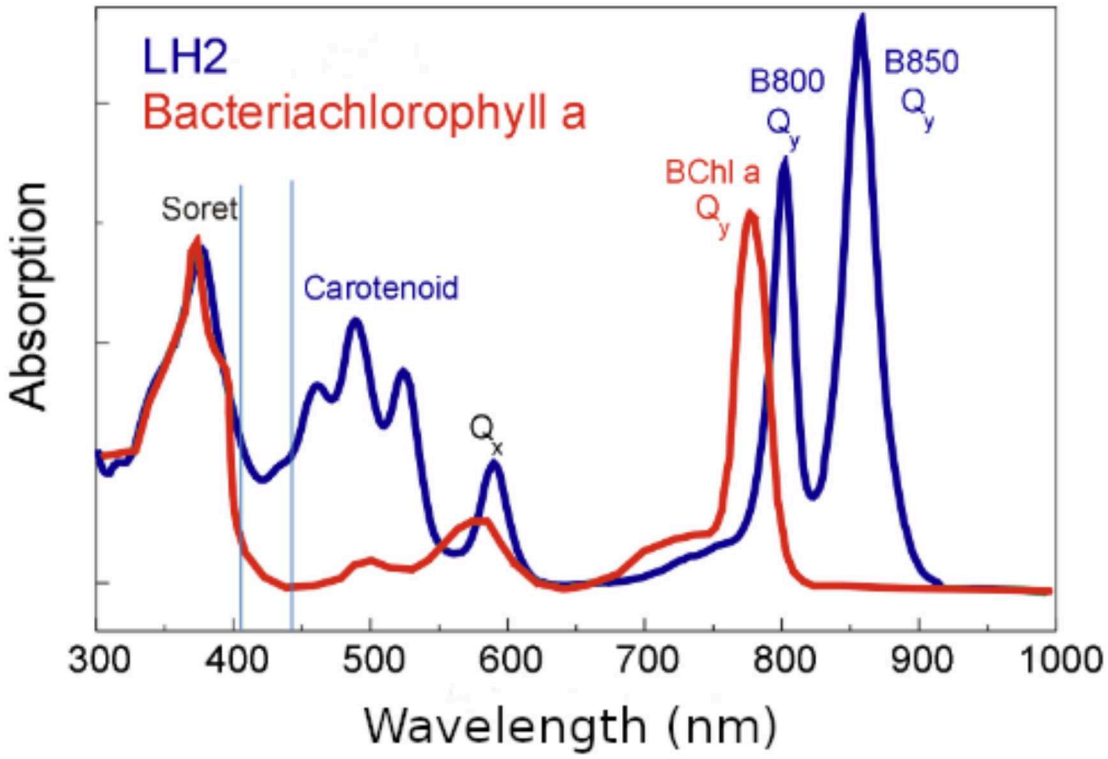

Figure 2.8: The absorption spectra of BChl *a* in an organic solvent in red) and of the LH2 complex. We see the presence of the Soret band around 350 nm for both. Carotenoids' absorption in LH2 is revealed around 500 nm. As we can see, normally BChl *a* in an organic solvent shares a similar Q_x with BChl *a*'s in LH2. However, there are two BChl *a*'s in the LH2 complex that has its Q_y red-shifted (800 nm for B000 BChls and 850 nm for B850 BChls) compared to the pigment in an organic solvent (around 770 nm) (Image modified from [Aegon, 2006]).

regular Förster energy transfer theory, spectral overlap between observable donor emission and acceptor absorption spectra allows for energy to be transferred, with the magnitude of that overlap, along with inter-pigment coupling, determining how fast the energy will be transferred. If there is an overlap between the emission and absorption spectra, Förster energy transfer is possible. In the case of extended Förster energy transfer theory, densities-of-states overlap is considered rather than spectral overlap, even though higher excitonic states of B850 BChls do not have oscillator strengths, as we saw previously. Transitions between B850 BChls are about a magnitude faster, in the 100 femtoseconds (fs) range [Berlin et al., 2007]. These transitions are in reality transitions between different delocalised excitonic states. Energy is transferred both within the individual LH2 and surrounding

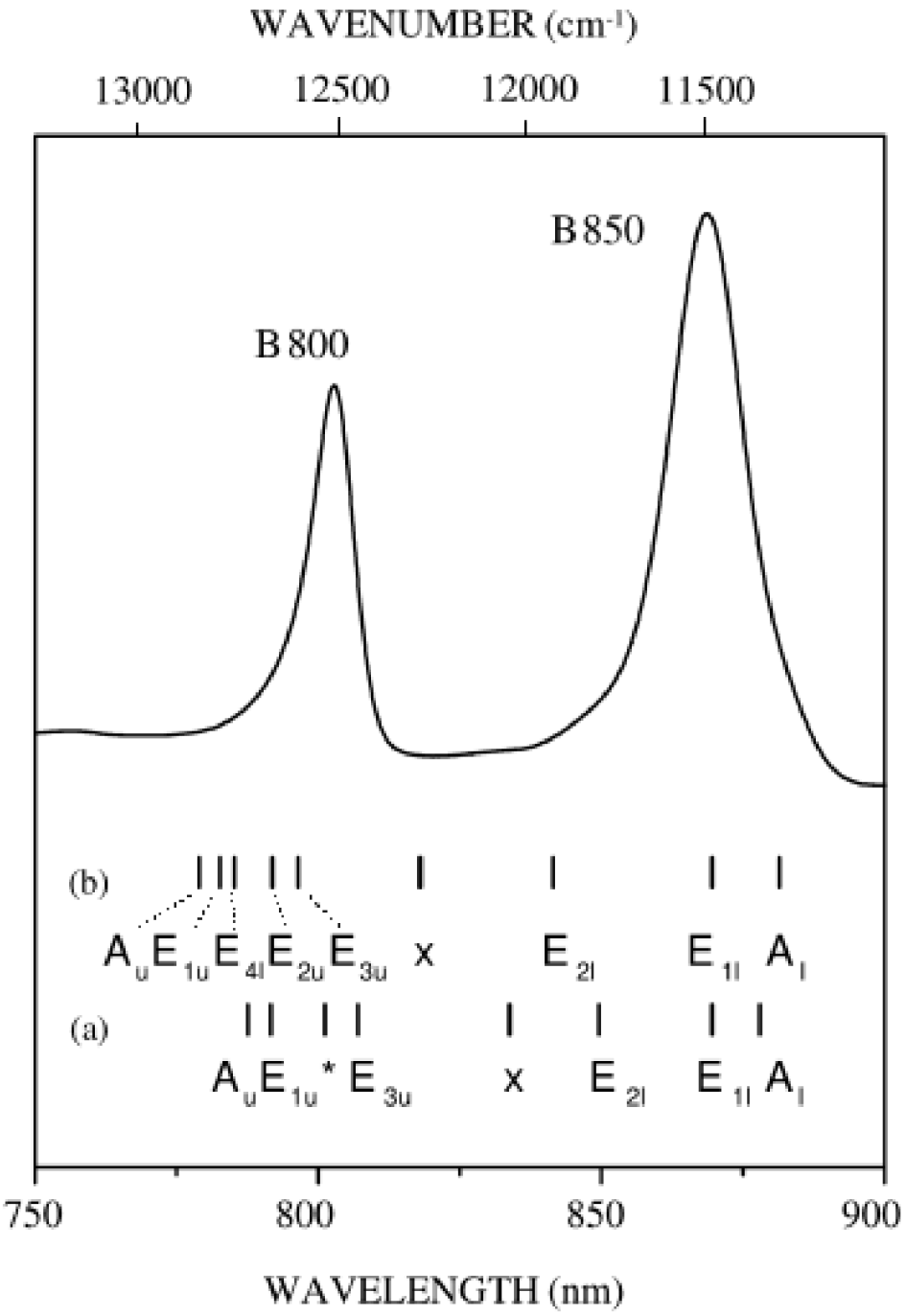

Figure 2.9: The absorption spectra of LH2 containing B800 and B850 BChls at 5 K with B850 ring exciton states denoted for a non-disordered system underneath. The (a) and (b) excitonic level structures were calculated with slightly varying parameters detailed in [Zazubovich et al., 2002].

LH2s. The amount of LH2s present in a bacterium can change depending on light and growing conditions, hence why it is sometimes referred to as the "variable" antenna complex [Kühlbrandt, 1995] [Cogdell et al., 1997].

2.2.4 Light-Harvesting Complex I (LH1) and Bacterial Reaction Centre (BRC)

Given that the energy proceeds in a "downhill transition", from 800 nm to 850 nm in the LH2s, it is eventually transferred to LH1 within several ps [Cogdell et al., 1997] [Zazubovich and Jankowiak, 2015]. LH1 is considered the core or inner antenna complex given its inner status in the PC and has a 68 Å inner space to accommodate the BRC [Kühlbrandt, 1995]. The LH1-to-BRC ratio is not influenced by light or growing conditions as seen in LH2 and hence, there is only a single LH1 and BRC [Kühlbrandt, 1995]. Similar to LH2, this complex also contains coaxial rings of α and β polypeptides consisting of n subunits with two highly-coupled B875 BChl *a*'s per subunit [Robert et al., 2003] [Zazubovich and Jankowiak, 2015]. The His acting as the ligands for the B850 BChls in LH2 are similarly present in LH1. However, due to slight differences in the chemical environment, the BChls are further red-shifted to 875 nm [Law et al., 2004]. Finally, the energy will be transferred to the BRC after approximately 35 ps [Zazubovich and Jankowiak, 2015].

The BRC is responsible for taking the light energy that has passed through the antenna complexes and make functional use of it in the Calvin cycle. The BRC is made up of three polypeptides, named the L, M, and H subunits [Williams and Allen, 2009]. The L and M subunits make up the core of the protein, whereas the H subunit is more peripheral. In the middle of the L and M subunits are ten cofactors involved in the transfer of electrons or energy. The cofactors are the following: two BChl *a* molecules forming a special dimer (P), which is similar to what we noted in PS I and PS II; two BChl *a* monomers (B_A and B_B); two bacteriopheophytins *a*'s (H_A and H_B); two ubiquinone molecules (Q_A and Q_B); a carotenoid molecule; and an iron atom [Williams and Allen, 2009].

Chapter 3

Spectral Hole Burning

In this chapter, we will examine the theory behind the technique of *spectral hole burning*. First, we will describe the spectral data we are interested in when it comes to chromophores, specifically the parameters of *zero-phonon lines*. Next we will explore the simplest manner of describing a pigment/protein system through the use of a *two-level system*, or *double-well potential*. We will introduce the technique of spectral hole burning, going into detail of *non-photochemical hole burning*. Finally, we will explore what non-photochemical hole burning can teach us about chromophore spectral data through *hole growth kinetics* and *hole recovery*.

3.1 Chromophore Spectral Data

3.1.1 The Franck-Condon Principle

When examining molecular movement, there exist molecular electronic transitions with accompanying changes in rotational and vibrational states [Gupta, 2016]. Thus, when examining the sum of molecular energy, there exist three components: electronic, rotational, and vibrational. In a similar fashion, we assume the wavefunction can be approximately described by all three motions:

$$\Psi(r, R) = \Psi_e(r, R) + \Psi_r(R) + \Psi_v(r) \tag{3.1.1}$$

where subscripts e, r, and v respectively denote electronic, rotational, and vibrational motion. The wavefunctions are in terms of r, the electronic coordinates, and R, the nuclear coordinates. Given the Born-Oppenheimer approximation, which comes from the fact that the mass of the nucleus is substantially larger than that of the electrons, the electronic motion is defined at an equilibrium nuclear distance (R_e) [Gupta, 2016]. Normally we assume that rotational motion comes from the nuclei alone; however, rotational motion is irrelevant in the case of frozen solutions, such as those used in our experiments.

When investigating the optical spectra of a chromophore, simultaneous electronic and vibrational transitions, referred to as vibronic transitions, give rise to the vibrational structure of the electronic bands of the system [Gupta, 2016]. The *Franck-Condon principle* allows us to describe these vibronic transitions, as well as the intensity of the vibrational structures [Gupta, 2016].

First, in the principle it is assumed that the potential well follows a parabolic shape and that the corresponding vibrational wavefunctions are regarded as those of quantum harmonic oscillators. Second, in similar fashion to that of the Born-Oppenheimer approximation, since the nuclei are so heavy and thus, nuclear motion is much slower than electronic motion, the nuclei can be considered stationary [Austin and Erramilli, 1995] [Gupta, 2016] [Ter-Mikirtychev, 2017]. Transitions are always vertical given this assumption. In order to determine the probability of finding an electron at a particular position x, we need only examine the vibrational wavefunction of the state's parabola. That is, transitions are most likely when there is a very good overlap of these wavefunctions in both the ground and excited electronic states. This is shown in Figure 3.1.

3.1.2 Zero-Phonon Lines (ZPLs) and Phonon Sidebands (PSBs)

In addition to the Franck-Condon principle, two other assumptions are introduced when examining chromophore spectra. First, the so-called *low-temperature approximation* is applied whereby electronic transitions only start at the lowest phonon level [Austin and Erramilli, 1995]. Second, *linear coupling* is assumed, whereby the harmonic oscillator potentials for both the ground and excited states are the same (that is, same

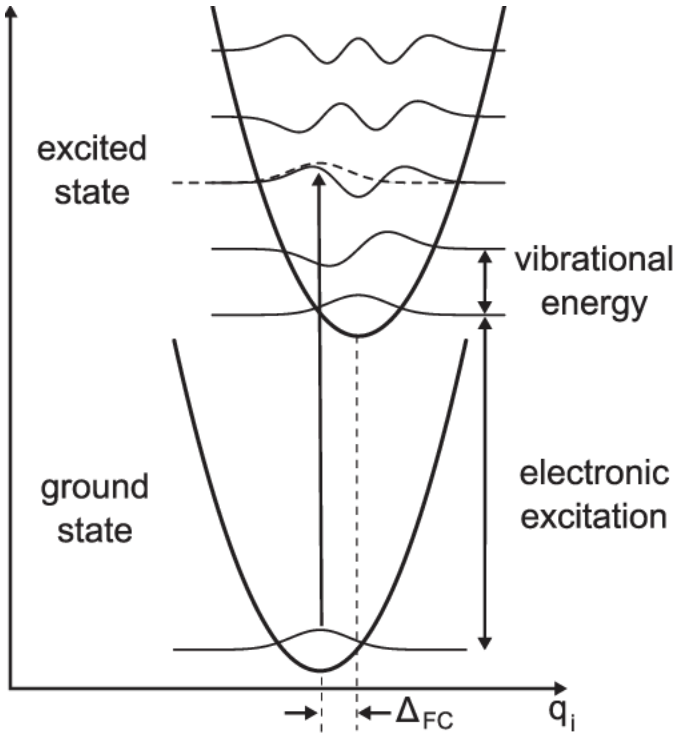

Figure 3.1: A depiction of the two parabolic functions of the ground and excited state with vibrational wavefunctions. This figure demonstrates only one wavefunction in the ground state, but there are many. Transitions can occur when there is a good overlap of the wavefunctions in the ground and excited state [Pittner et al., 2013].

curvature and frequency), though, of course, they may be shifted differently along the generalised coordinate [Berlin et al., 2006]. Having similar parabolas for both the ground and excited states means vibrational frequencies are the same in absorption and in emission. This principle and these assumptions allow for transitions to be examined, with the overlap of the vibrational wavefunctions being the main contributor for possible transitions. In the end, these transitions are transcribed into the chromophore spectral data in terms of frequency and are referred to as *zero-phonon lines* (ZPLs) and *phonon sidebands* (PSBs), also known as phonon wings (PWs).

The ZPL refers to the electronic transition in the system whereby no change in phonons is observed (that is, from the lowest vibrational level in the ground state to the lowest vibrational level in the excited state) [Sapozhnikov, 1978] [Ter-Mikirtychev, 2017]. The PSB refers to the various electronic transitions accompanied by excitation of phonons [Sapozhnikov, 1978]. The ZPL is a sharp peak with a width Γ_{hom} where its relative intensity

is defined by the Debye-Waller factor

$$\alpha = \frac{I_{ZPL}}{I_{ZPL} + I_{PSB}} = e^{-S(T)} \tag{3.1.2}$$

where I_{ZPL} and I_{PSB} are the integral intensities of ZPL and PSB respectively [Friedrich, 1995] and $S(T)$ is the Huang-Rhys factor which describes the coupling strength between the electrons and phonons in the system [Sapozhnikov, 1978].

3.1.2.1 Factors Influencing the ZPL and Homogeneous Broadening

The widths of the ZPL are determined by the lifetimes of the excited states, meaning they reveal information about pure dephasing, energy transfer, and charge transfer. This makes ZPL particularly important in photosynthesis research. However, the intensity, width, and location of the ZPL are influenced by various other factors. Temperature of the system is one pertinent factor which affects the intensity and width of the ZPL, as shown in Figure 3.2 [Sapozhnikov, 1978] [Friedrich, 1995]. With decreasing temperatures approaching 0 K, the ZPL optimally displays its characteristic sharp and narrow peak. However, as temperature increases, the ZPL's peak intensity decreases due to the width Γ_{hom} increasing substantially and differentiation between the ZPL and PSB is impossible after approximately 50 K [Friedrich, 1995].

Another important factor is the electron-phonon coupling strength, which we saw with the Huang-Rhys factor in Eq. 3.1.2. If electron-phonon coupling is weak, that is, $S < 1$, then the ZPL is strong and the PSB is relatively small. If electron-phonon coupling is strong, that is, $S > 1$, then the ZPL is minimised and the PSB is relatively more intense [Sapozhnikov, 1978].

Finally, interactions within the environment of the system can cause shifts of the ZPL lines. Pure dephasing due to scattering of phonons and, thus, quadric electron-phonon interactions, can cause line broadening. This is equivalent to saying that, when the shifts are small (that is, smaller than the ZPL width) and frequent, they will contribute to the observable ZPL width. However, when the shifts are large, they cause bigger problems. When examining a macroscopic sample, while it is assumed that identical chromophores

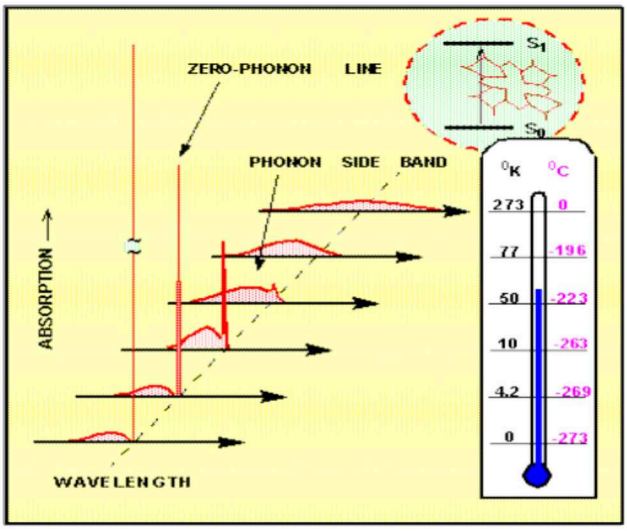

Figure 3.2: Temperature has an important effect on the intensity and width of the ZPL. As temperature decreases, the ZPL's prominence increases, with a decreased Γ_{hom} width, and it is much easier to identify. Consequently, experiments were performed close to absolute zero to optimise the ZPL [Rebane, 2008].

will have identical optical spectra with overlapping ZPLs and PSBs, this is rarely the case. Instead of observing so-called homogeneous lines, large shifts due to interactions in the environment, such as in PCs, make way for *inhomogeneous broadening* (width of Γ_{inh}). This means ZPLs and their accompanying PSBs are shifted and, therefore, are impossible to decipher individually. See Figure 3.3 for details.

3.2 Two-Level System (TLS)

The energy landscape of functioning proteins is a complicated affair. Rather than remain static, proteins shift into varying conformational substates depending on thermodynamic fluctuations [Frauenfelder et al., 1991] [Ramanathan et al., 2013]. These conformational substates can be imagined as the troughs throughout the energy landscape, with varying barriers surrounding them [Frauenfelder et al., 1988]. Substates can come from different protein folding and heterogeneous interactions with the environment [Ramanathan et al., 2013]. The energy landscape is hierarchical in nature, referred to as a *folding funnel* with higher and lower tiers where molecules can reside, as seen in Figure 3.4 [Frauenfelder et al., 1991] [Zazubovich and Jankowiak, 2015]. However, when working

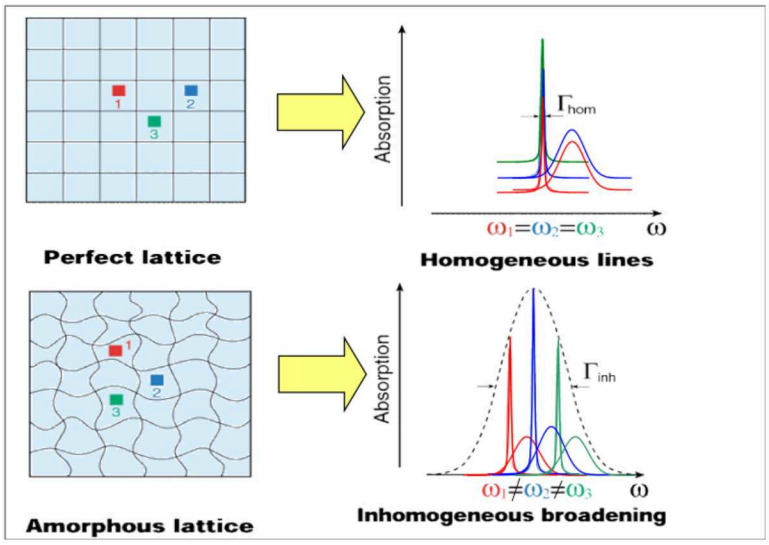

Figure 3.3: Similar chromophores should have overlapping ZPLs and PSBs as in the case of the perfect lattice (depicted on the top). In real life, we often work with amorphous lattice situations (as depicted on the bottom). In this case, the ZPLs' width, intensity, and location are different and lead to what we call inhomogeneous broadening.

at low temperatures, molecules are unable to jump higher tiers and are instead only allowed movement in lower tiers [Zazubovich and Jankowiak, 2015].

Consequently, it seems futile to attempt to describe these complex system accurately. However, there is often a simple way to describe these energy landscapes through what is designated a *two-level system* (TLS) or *double-well potential* (see Figure 3.5). Originally used to describe the energy landscapes of glasses [Anderson et al., 1972], the model has also been found to work for proteins [Frauenfelder et al., 1988]. In this case, rather than a varying degree of hills and troughs, there exist two conformational substates along a generalised or conformational coordinate [Ramanathan et al., 2013] [Najafi et al., 2015]. This means that, when examining the TLS, the two major wells are two relevant substates which describe a single protein frequenting these potential wells. The two substates, henceforth referred to as wells, have varying, asymmetrical depths defined by the asymmetry parameter Δ and with an energy barrier V. Thus, in order for a transition to occur between the two wells, the proteins in question have structural elements that either barrier-hop or tunnel through the barrier of height V. At low temperatures, tunnelling is the predominant mechanism involved. The tunnelling parameter (known as λ) is defined as

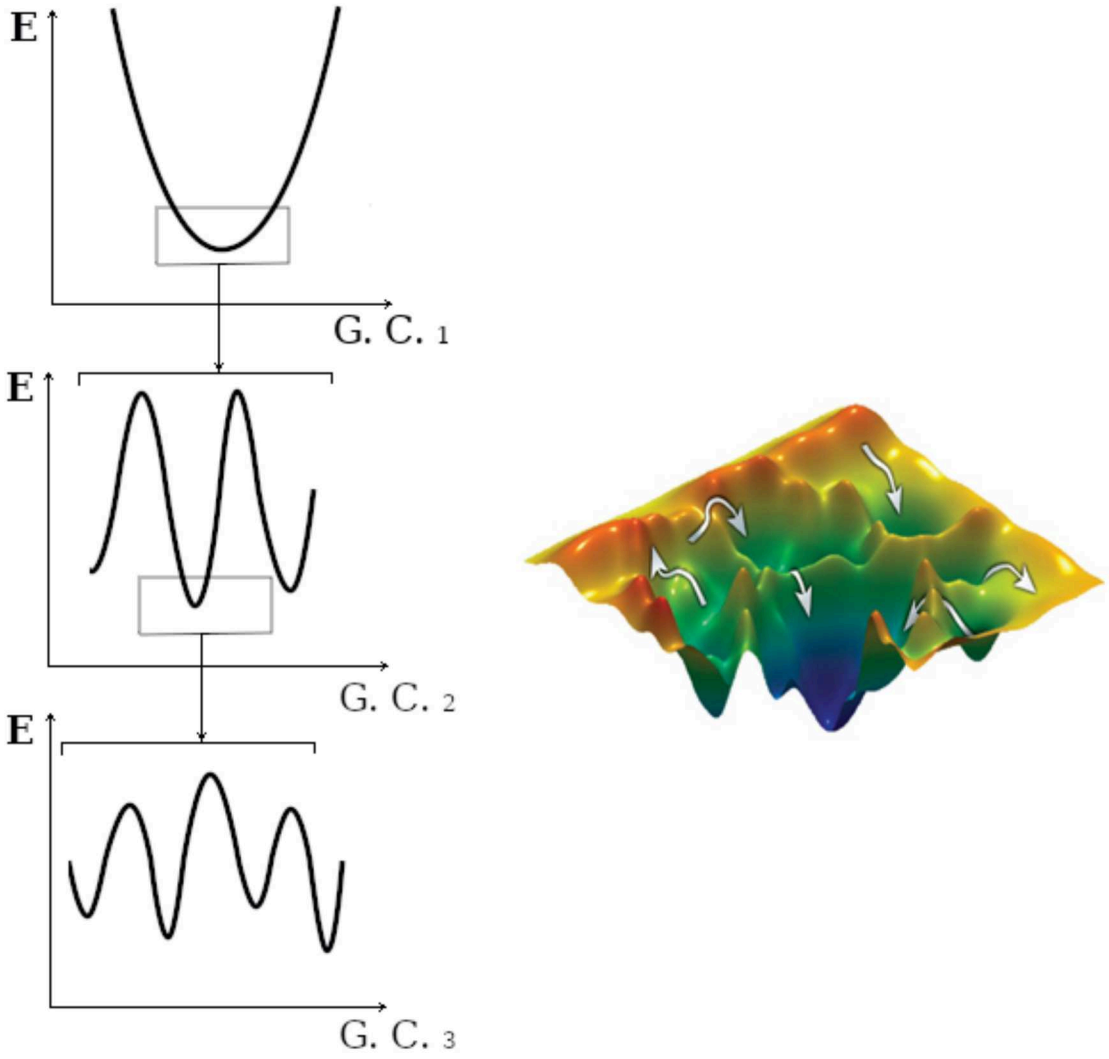

Figure 3.4: The folding funnel of the energy landscape where "G. C." stands for generalised coordinate. The one-dimensional representations of the substates are on the left (with lower and lower tiers as we move down the figure) and the lower, two-dimensional tier representation is on the right. As we delve into lower and lower tiers, the energy landscape becomes more diverse. At very low temperatures, molecules are limited to movement only in the lowest tiers. It's important to note that substates are, in reality, multidimensional. That is to say, there may be more than one generalised coordinate (see [Shafiei et al., 2019] from our group on NPHB on two tiers of the protein energy landscape) (Right image from [Pirchi et al., 2011]).

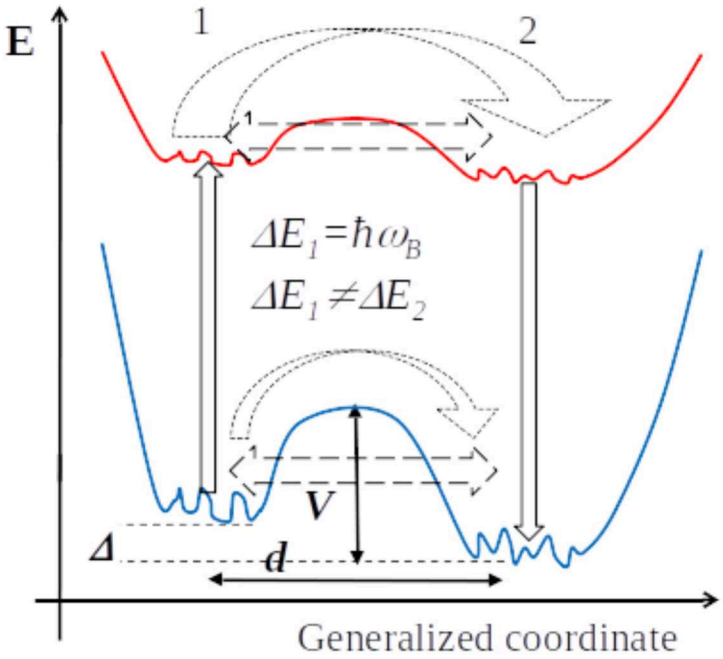

Figure 3.5: The two-level system (TLS), also known as the double-well potential, is the simplest manner of describing the energy landscape of a PC component. The blue potential represents the electronic ground state and the red potential represents the excited state. The **1** corresponds to the first well and the **2** corresponds to the second well. Δ is the difference between the two ground state wells; V is the potential energy barrier height; and d is the distance between the ground state minima in a generalised coordinate. Pigments can become excited into excited well 1 from ground well 1 or back down to the ground state via excited well 2 as shown by the arrows. The dotted arrows represent barrier hopping whereas the dashed arrows represent tunnelling through the barrier potentials. As one can see, the potential energy barrier height for the ground state is taller than in the excited state, increasing the probability that the pigments will tunnel through the barrier in the excited state rather than in the ground state. The tiny structures at the bottom of each well represent the lowest tier of the energy landscape previously discussed. They are actually responsible for ZPL broadening, which are essentially shifts by an amount smaller than the ZPL width [Najafi et al., 2015].

$$\lambda = \frac{d}{\hbar}\sqrt{2mV} \tag{3.2.1}$$

where d is the distance between the well minima in the generalised coordinate, m is the effective mass of the involved atoms/proteins, and V is the energy potential barrier height already defined [Najafi et al., 2012] [Zazubovich and Jankowiak, 2015]. This particular formula corresponds to a rectangular barrier where d is the barrier thickness. Thus, using this formula for our double-well potentials is an approximation.

The TLS model used in optical spectroscopy has an additional component when describing chromophore optical data: rather than be a single double-well potential, an excited state potential is added to the system to create a two-double-well system [Zazubovich and Jankowiak, 2015]. This means pigments in the ground state have the opportunity to become excited and go into a higher potential. Likewise, they may also go back down into the ground state. We will further explore this dynamic in Section 3.3.1.

3.3 Spectral Hole Burning (SHB)

In Section 3.1.2.1, it was stated that inhomogeneous broadening results in ZPLs of similar chromophores being shifted in a manner that makes one incapable of identifying them individually. As well, in Section 3.2, it was noted that, while the energy landscape can be hierarchical in nature and difficult to describe, it is possible to describe them rather simply with the use of a TLS. Through the use of a technique called *spectral hole burning* (SHB), however, it is possible to use this TLS system to find the hidden ZPLs. Crudely describing it, the technique involves burning a hole in the absorption spectra at a particular resonant frequency to reveal the ZPL.

This technique can be sub-divided into two different methods: *photochemical hole burning* (PHB) and *non-photochemical hole burning* (NPHB). For PHB, the molecules at a particular resonant frequency with the laser are photo-transformed. That is, these molecules are unable to become excited at the resonant frequency given a chemical change unlike those not at the resonant frequency. Consequently, this means a hole appears in the spectral data which mirrors the ZPL at that resonant frequency.

For NPHB, rather than the molecule itself being transformed, the environment is altered [Zazubovich and Jankowiak, 2015]. This, in turn, alters the ZPL frequency since molecule-environment interactions are different. Once again, a hole is left in the spectra with the mirrored ZPL (so called ZPH, or *zero-phonon hole*) showing up as a hole in the distribution along with the corresponding mirrored PSB (or *phonon-sideband hole*, PSBH). This technique works for all amorphous solids. In our experimental work, NPHB was used and thus, a detailed explanation of the process will be provided in Section 3.3.1.

3.3.1 Non-Photochemical Hole Burning (NPHB)

As mentioned previously, the environment rather than the molecule is altered in the case of NPHB. The process can be described rather simply by examining the Figure 3.5. It should be stressed that NPHB is a low-temperature spectral technique. As mentioned in Section 3.1.2.1, the ZPL has the most pronounced shape at low temperatures, so NPHB should be conducted at low, liquid-Helium temperatures. And as was mentioned in Section 3.2, tunnelling is the predominant phenomenon observed at low temperatures, particularly under 10 K, which will be important when describing NPHB [Zazubovich and Jankowiak, 2015]. Therefore, NPHB is normally used at low temperatures.

When we are conducting NPHB experiments, rather than examine a single pigment/protein system, we are looking at an ensemble of pigments in protein systems. Due to disorder from these pigment/protein systems, the parameters of the individual TLS are picked from certain distributions, meaning they are somewhat random. During these NPHB experiments, if we describe the distributions of the transition rates by the first approximation alone, then only the V distribution describes the transition rate. With increasingly better approximations, distributions of asymmetry, distance between the minima, and even the effective mass of the involved pigments/proteins (assuming we are dealing with cooperative effects, like several hydrogen bonds rearranging in concert) could have an effect.

Beginning in the first ground state well, the pigments in the PC are excited into the first excited well. From there, the pigments may tunnel through the potential energy barrier (which is much lower than the one in the ground state) in order to pass into the excited

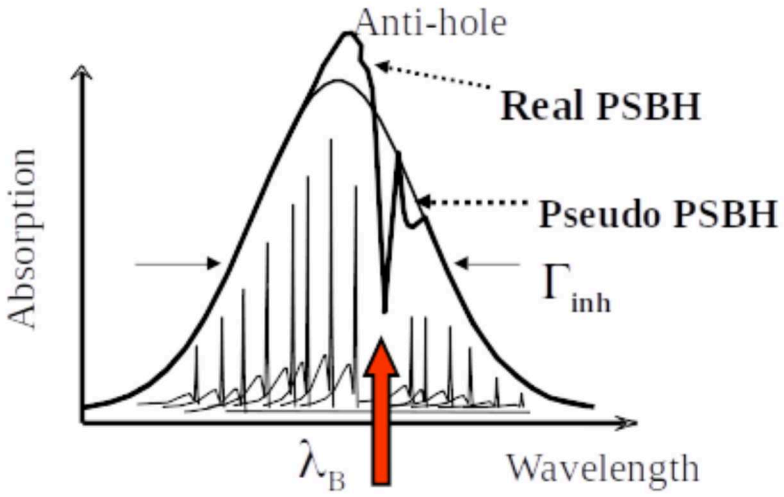

Figure 3.6: The NPHB absorption spectra with ZHB pointed out with red arrow found in the inhomogeneously broadened hole. As can also be seen, an anti-hole forms as the pigment is now residing in a different ground state, causing an over-representation at a different wavelength. The real PSBH is the accompanying PSB from the ZPL. The pseudo PSHB is due to the hole being burnt into the PSB rather than the ZPL, meaning the pigments become excited through the PSB and lead to a "pseudo" hole [Shooshtari, 2013].

state's second well. Finally, the pigments will eventually lose energy and go back down into the ground state, though now, they will fall into the ground state's second well. This second well is what is meant by altered environment as the pigments are now residing in a different area of the generalised coordinate

The NPHB absorption spectra (as shown in Figure 3.6), apart from the obvious hole created by the hole burning process, also has what is called an anti-hole. The anti-hole refers to the fact that now a larger amount of pigments are residing in the ground state second well. Consequently, they lead to an over-representation of specimens at a different frequency, shown as an anti-hole. There is also the demonstration of a "real PSBH" and "pseudo PSBH". While the real PSHB shows the corresponding PSB from the single-molecule spectra, the pseudo PSBH comes from the laser frequency not necessarily falling directly on the ZPL. That is, the pigments are excited through the PSB rather than through the ZPL and produce this feature.

How can one ensure that generally, the pigments tunnel through the excited state rather than in the ground state? In most amorphous systems, the barrier height in the excited

state is much lower than that in the ground state, allowing for the pigments to cross it with a higher probability in their excited state lifetimes compared to the probability of tunnelling in the ground state [Zazubovich and Jankowiak, 2015]. On that note, it is possible to describe the NPHB yield ϕ in terms of the tunnelling parameter λ noted in Eq. 3.2.1 through the following formula

$$\phi(\lambda) = \frac{\Omega_0 exp(-2\lambda)}{\Omega_0 exp(-2\lambda) + \tau_{fl}^{-1}} \tag{3.3.1}$$

where Ω_0 is the attempt frequency is on the scale of (10^{12} Hz), which describes how often the system attempts to tunnel through the barriers, and τ_{fl} is the fluorescence lifetime without excitation energy transfer (EET) present and without dephasing (where dephasing is the process in which phonon scattering alters the phase of the excited electronic state wavefunction without getting the pigment to the electronic ground state) [Najafi et al., 2015]. Since the pigment stays in the excited state, it still can tunnel through the excited state barrier.

It is also possible to describe the final post-burn spectrum $D(\Omega, t)$ after illumination at a specific frequency ω_B at time t via the NPHB master equation, which is defined as [Najafi et al., 2012]

$$D(\Omega, t) = \frac{3}{2}\int d\omega L(\Omega - \omega)G(\omega)\int d\lambda f(\lambda)\int d\alpha \sin\alpha \cos^2\alpha e^{-P\sigma\phi(\lambda,\tau_{fl})L(\omega_B-\omega)t\cos^2\alpha} \tag{3.3.2}$$

where $G(\omega)$ is the site distribution function, describing the probability of a specific chromophore with a ZPL at a laser frequency in the inhomogeneously broadened distribution; $f(\lambda)$ is the distribution describing the tunnelling parameter λ from Eq. 3.2.1; α is the angle between the electric field $\boldsymbol{E}$ of the light and the transition dipole moment vector $\boldsymbol{\mu}$ of the chromophore, representing the random isotropic orientation of the chromophores in the equation; P is the photon flux; σ is the integral absorption cross-section; ϕ is the NPHB yield from Eq. 3.3.1; and $L(\omega)$ is the single-site spectrum (normalised to the area = 1 on the ω scale) which contains information about the ZPL and PSB [Reinot and Small, 2000].

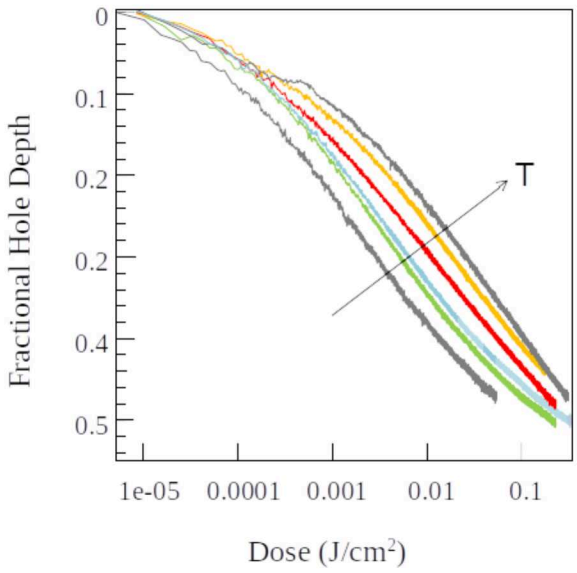

Figure 3.7: An example of what HGK can show us. Here, using cytochrome b_6f, we can see that hole growth slows down with increased temperature, therefore allowing us to recognise a temperature-dependence for HGK. These curves were obtained with relatively low light intensity, low enough to ignore triplet-related effects (see next chapter) [Najafi et al., 2015].

3.3.2 Hole Growth Kinetics (HGK)

In order to better understand final post-burn spectra, one can also examine the *hole growth kinetics* (HGK), or how a hole burns while it is burning. The process involves choosing a particular frequency to burn at, the resonant laser frequency ω_b we previously described, and increasing the irradiation dose at that frequency (in the case of HGK, this means burning the hole for longer and longer times at the same intensity). This will lead to lower and lower absorption in the sample, which leads to a hole. Thus, through HGK, it is possible to infer how deep a final saturated hole will be and determine the Huang-Rhys factor S. One can also observe HGKs in order to make possible conclusions about how other factors can affect how a hole burns. For example, as was previously found by [Najafi et al., 2015] and shown in Figure 3.7, temperature can easily affect the speed of burning, with higher temperatures slowing down HGK curves. Furthermore, the HGK curve is usually fitted to obtain the distribution of tunneling parameter λ in the excited state.

3.3.3 Hole Recovery

Another interesting experimental procedure involved with NPHB is examining hole recovery, or how a hole recovers over time. There are two main types of hole recovery experiments. The first is *fixed-temperature recovery* whereby the hole is observed over time at a low, fixed temperature. This means that tunnelling in the ground state TLS is the phenomenon observed with fixed-temperature recovery. These experiments are lengthy and potentially costly, however, given that full recovery could take up to a week at 5 K.

The second type is *thermocycling*, whereby the hole recovers at varying, increasing temperatures (see Figure 3.8). First the hole spectrum is recorded at the burn temperature (at 5 K). The temperature is then raised to a higher peak temperature before being lowered back down to the burn temperature to record a new hole spectrum. This cycle continues with greater and greater peak temperatures used over time. It should be noted that, at increased temperatures, tunnelling and barrier hopping both help in the recovery process. Eventually, at high enough temperatures, barrier hopping dominates. Consequently, in this technique, we are not examining the distribution of our tunnelling parameter λ in the ground state, but instead the distribution of our barrier, V. Therefore, by comparing fixed-temperature hole recovery and thermocycling results, we can make conclusion about "md^2", that is, examine the conformational coordinate, allowing us to make conclusions about the nature of the protein contributing to the conformational changes/the TLS itself.

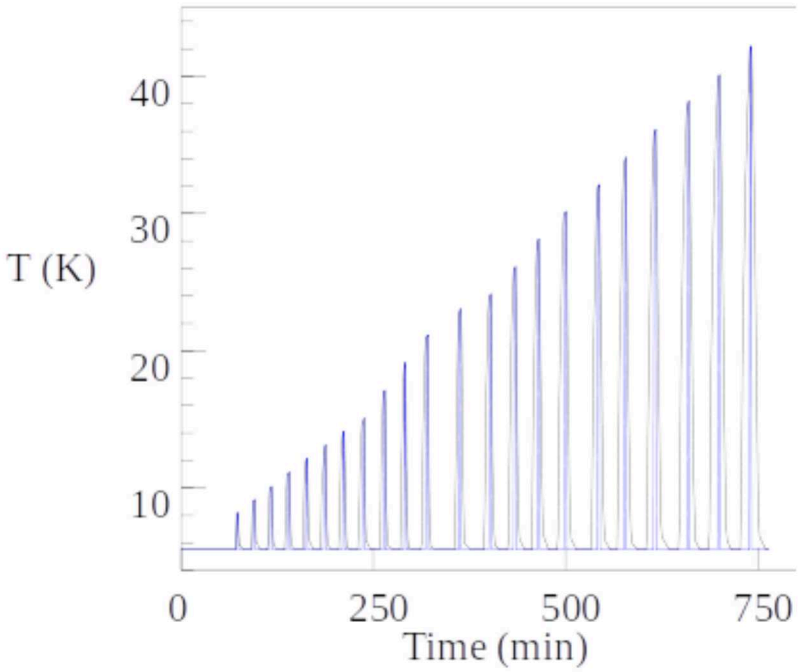

Figure 3.8: Thermocycling is a hole recovery process whereby temperature is slowly increased overtime while observing the hole at the initial, low temperature to optimise the ZPL. This allows for a faster recovery time compared to fix-temperature recovery. The two curves correspond to the same experiment, but with different precision of temperature in relation to time.

Chapter 4

Experimental Research

In this chapter, we report the experimental research brought on by a paper published from our research group in part on the solvent deuteration effects on cytochrome b_6f [Levenberg et al., 2017]. First we will explain the motivation brought on by [Levenberg et al., 2017], specifically the question of whether or not local heating could explain the deuteration effect noted for the cytochrome b_6f sample. Then we will explain the new complex created in order to test our hypothesis, a modified LH2 containing an arbitrary amount of Chls. We will briefly explain the methodology involved in creating the modified LH2, as well as the instruments used and experiments performed. We will then explain the results we observed, specifically our attempt at detecting illumination-intensity dependence in our modified LH2 sample, our observation of EET-capable and EET-incapable Chls in our samples, our use of simulated triplet states to explain discrepancies observed in supposed hole depths from HGK curves and actual hole depths, and the potential discovery through thermocycling of pigment participation in the generalised coordinate.

An in-depth paper on our modelling of triplet states has also been published this year [Trempe et al., 2021].

4.1 Introduction

4.1.1 Motivation

In a previous paper published by our research group from [Levenberg et al., 2017], one focus of the work was to determine if solvent choice, particularly the switch from a protonated to a deuterated solution, could affect SHB results in the cytochrome b_6f complex. It had been previously shown that, in aluminum phthalocyanine tetrasulfonate (ATP) for example, deuteration of the solvent led to a 50-fold decrease in hole burning yield [Kim et al., 1996]. Conversely, partial deuteration of $NaMgAl(oxalate)_3 \cdot 9H_2O/Cr(III)$ showed increased efficiency in hole burning [Riesen and Hughes, 2003]. Therefore, the purpose was to observe differing spectral dynamics of cytochrome b_6f in a deuterated solvent compared to a regular, protonated solvent. In other words, we wanted to see if the light-triggered dynamics observed in our NPHB experiments were dynamics of the protein or of the surrounding solvent.

In the end, hole burning and recovery data revealed that the tunnelling parameter λ did not depend much on the deuteration of the solvent, not as much as changing the effective mass by 2 would lead to. With increased temperatures, hole burning slowed down overall. This was expected, with temperature dependence previously noticed in Figure 3.7 [Najafi et al., 2015]. Interestingly, however, an illumination-intensity dependence was seen predominately in the deuteration-solvent sample. As seen in Figure 4.1, the protonated-solvent sample has overlapped HGK curves with different illumination intensities; however, the deuterated sample clearly shows a slowing down of the HGK with increasing illumination intensity in the same intensity range. While the phenomenon is demonstrated for 5.5 K in the figure, it was observed at different temperatures as well.

This illumination-intensity dependence was a perplexing observation. Faster burning for higher intensities would be the expected observation when examining the HGK in terms of J/cm^2 (as done in Figure 4.1) since the same number of photons are delivered in a shorter amount of time, favouring the likelihood of burning over recovery [Levenberg et al., 2017]. Even after taking into account the obvious effect that higher dose should lead to more hole burning, intensity increase still seemed to slow down hole burning. Thus, why a slowdown

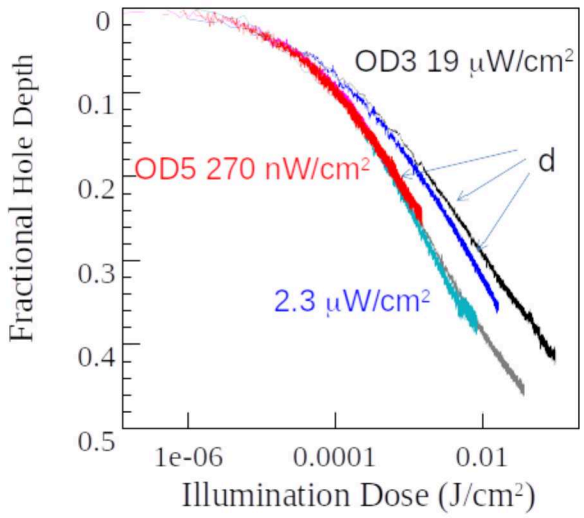

Figure 4.1: The observed illumination-intensity dependence in the HGK curves of cytochrome b_6f for the deuterated sample versus the protonated sample at 5.5 K. Three different illumination intensities were used for each sample. The protonated sample curves are the magenta (with illumination intensity of 270 nW/cm^2), cyan (2.3 μW/cm^2), and grey (19 μW/cm^2). The deuterated sample curves are red (270 nW/cm^2), blue (2.3 μW/cm^2), and black (19 μW/cm^2). 0.001 J/cm^2 corresponds to around 50 seconds with an illumination intensity of 19 μW/cm^2. As shown, the protonated sample has overlapped HGK curves even as intensity is increased, but the deuterated sample has slower HGK curves with increasing intensity [Levenberg et al., 2017].

with higher intensities and why so prominently displayed in the deuterated sample?

The hypothesised reason came from the temperature dependence observed in cytochrome b_6f. As already stated, it was noticed earlier that in many complexes, including CP43 and cytochrome b_6f (where Chl molecules are far away from each other, resulting in weak energy transfer between them), present in a protonated environment showed a slowdown in their hole burning as temperature increased [Najafi et al., 2012] [Najafi et al., 2015]. Therefore, local heating (that is, heating of the immediate environment of the protein by several Kelvin compared to the whole sample's temperature) in the deuterated sample could explain the slowing down of the HGK curves. Given that deuterated substances have somewhat lower heat conductivities compared to their respective protonated substances, local heating could explain why the deuterated sample was affected but not the protonated one. Subsequent analysis of available literature showed that bulk heat conductivity of both protonated and deuterated water-glycerol mixtures is too high to explain local heating by

several Kelvin with light intensities employed in our experiments [Levenberg et al., 2017]. Thus, it was suggested that it may be the interface heat conductivity (that is, between the normal/regular/still-protonated protein and the deuterated solvent) rather than bulk conductivity that may be responsible for the observed intensity effect and its deuteration dependence. Therefore, with all this in mind, this led us to try and more rigorously verify if local heating was the reason behind this illumination-intensity dependence observed in the deuterated sample.

4.1.2 Modified LH2

In order to test the local heating hypothesis, it is necessary to control whether or not local heating by illumination is present. That way, if we observed HGK of the chlorophyll when it was being heated and when it was not, we could note if it had the temperature dependence we expected. As previously discussed in Section 2.2.3, the transition between B800-B850 BChls in LH2 results in dissipation of a significant amount of heat, equivalent to approximately 1000 cm^{-1} per absorbed photon. This means if the sample was illuminated at 800 nm, energy would transfer between B800 and B850 BChls and result in heat, meaning we could control the local heating in the sample. Consequently, a so-called modified LH2 (see Figure 4.2) was used whereby an arbitrary amount of B800 BChls in LH2 were replaced with Chls. This would allow us to observe low-intensity HGK at approximately 670 nm, the absorption wavelength corresponding to Chls, while either illuminating or not illuminating the sample at 800 nm, corresponding to the BChls. Simply put, the Chls would act as thermometers, reacting to the controlled local heating from the BChls.

4.2 Methodology

Dimeric cytochrome b_6f obtained from spinach was isolated by Dr. Rafael Picorel, with an explanation of the sample in [Najafi et al., 2015]; this sample was also used in [Levenberg et al., 2017]. The samples were solubilised in n-octyl β-D-glucopyranoside (OGP) detergent, though similar results were seen when samples were solubilised with dodecyl β-D-maltoside.

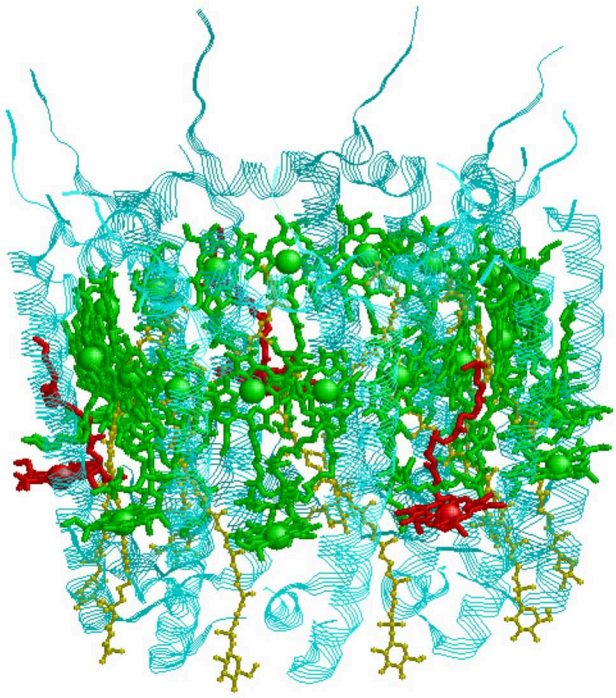

Figure 4.2: A modified LH2 was used in our experiments. An arbitrary amount of B800 BChls, shown in green, were replaced with Chls, shown in red, allowing for the Chls to act as thermometers when the sample was illuminated at 800 nm given consequential heat dissipation from the B800-B850 transition.

LH2 from *R. acidophilus* was used as our so-called regular LH2 and was the basis for the modified version, both also supplied by Dr. Rafael Picorel. In the modified version, an arbitrary amount of B800 BChls were replaced by Chls. The technique, which was based on [Fraser et al., 1999], will be summarised here.

First, desired LH2 concentration was achieved by diluting the complex in a 1:10 solution with 20 mM Tris-HCl (which has a pH of 8.0) and 1% (v/v) Triton TBG10. Next, acetic acid was added to decrease the pH of the solution to 5 and allow for the release of some of the B800 BChls. In order to determine how many B800 BChls were released from LH2, an absorption spectrum was taken. Decreased peaks at 800 nm and increased peaks at 770 nm meant some of the BChls were freed from the complex, given that BChls in organic solvents have a peak absorption around 770 nm rather than 800 nm. Once a certain quantity of BChls were dislodged from the complex, the mixture was added to a phosphocellulose column in 20 mM of potassium phosphate (pH 4.75). In order to remove the free-floating

or weakly-bound BChls, the column was washed with 20 mM potassium phosphate and 1% (v/v) TBG10 until the eluant had minimal absorption peaks at 770 nm (<0.01). The B850-heavy complexes were then exchanged into dodecyl β-D-maltoside (that is, a different detergent than the 1% TBG10 used previously) by washing the column several times with 20 mM potassium phosphate and then another several times with 20 mM potassium phosphate and 0.1% (w/v) LM until the eluant had minimal absorption peaks at 770 nm (<0.01). This ensured that no free-floating or weakly-bonded BChls were left in the mixture. Finally, the B850-heavy complexes were eluted with 500 mM potassium phosphate and 0.1% (w/v) LM. Further purification was performed and the best resulting B850-heavy complexes were collected.

In order to reconstitute the previously occupied B800 sites with Chls, the now B850-heavy complexes were diluted with 20 mM potassium phosphate and 0.1% (w/v) LM to obtain a BChl concentration of 9 μM. A certain volume of Chls dissolved in methanol was added to the mixture to obtain a final concentration of 15 μM. KOH was added to adjust the pH to 8 and the sample was gently shaken for two hours at room temperature. Finally, the sample was concentrated and their absorption spectra were recorded. The samples were again purified from free-floating unattached Chls and BChls by chromatogaphic methods. See Figure 4.3 for resulting absorption spectra of unmodified and modified LH2 samples used in our experiments.

Prior to the experiment, the protein solution was mixed with glycerol which aided in forming a transparent glassy solid at our near-absolute-zero experiments and acted as a cryoprotectant as well. A D_2O-based buffer and special d_8-glycerol, where 98% of protons are exchanged for deuterons, from C/D/N Isotopes were used for the deuterated solvent samples. Samples spent minimal time at room temperature to limit deuteration of the proteins themselves. They were placed inside a liquid helium optical cryostat. High-resolution spectra and HGK curves were measured using fluorescence excitation mode with a SpectraPhysics/Sirah Matisse-DS frequency-stabilized tunable dye laser (bandwidth of approximately 0.15 MHz). Fluorescence was detected through the use of a Hamamatsu photon counting module with a combination of long-pass (AELP700; Omega Filters, VT) and short-pass (750 nm, ThorLabs) filters.

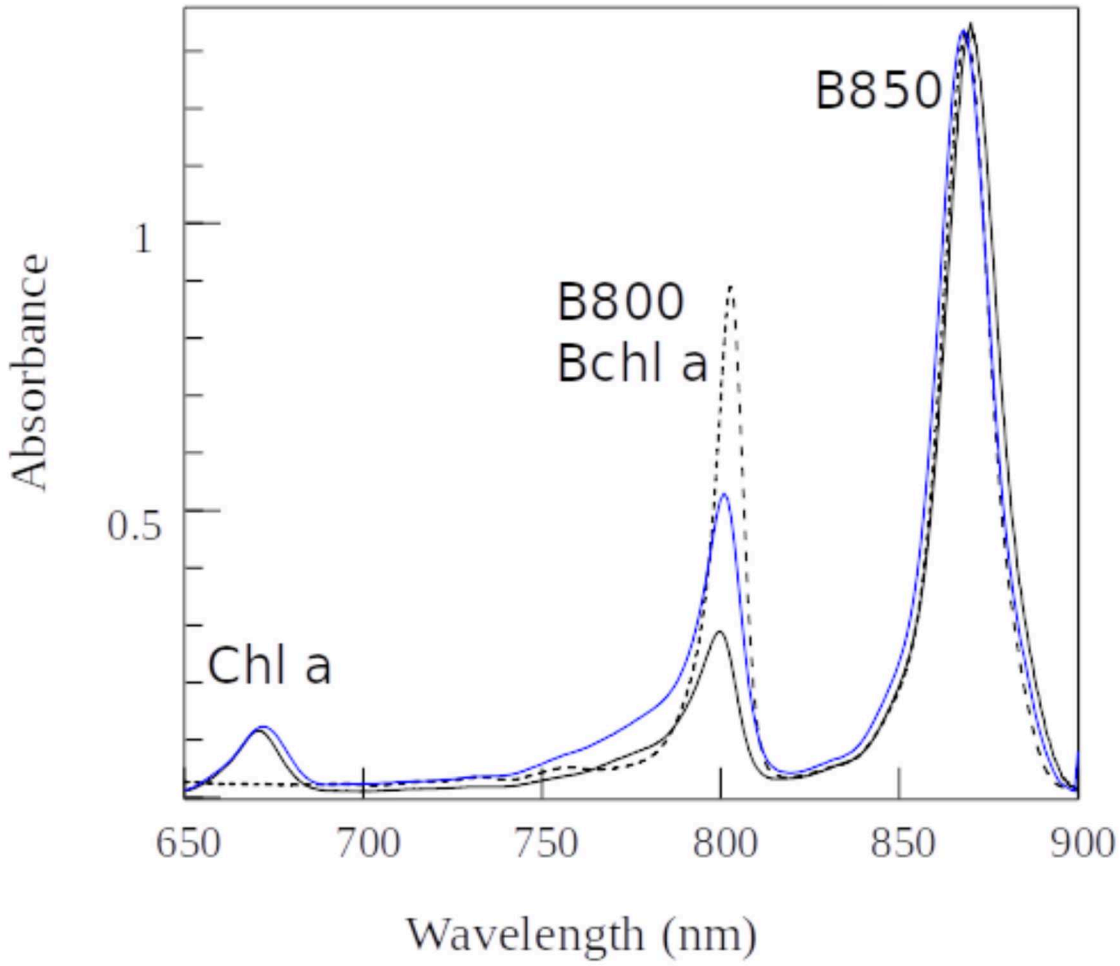

Figure 4.3: The absorption spectra at 5 K of our LH2 samples. In dashed black, we have our regular LH2 before modification. In solid black, we have our older protonated-solvent sample of modified LH2. In blue, we have our deuterated-solvent sample of modified LH2. The spectra were normalised at B850, with the Chl band being similar a coincidence.

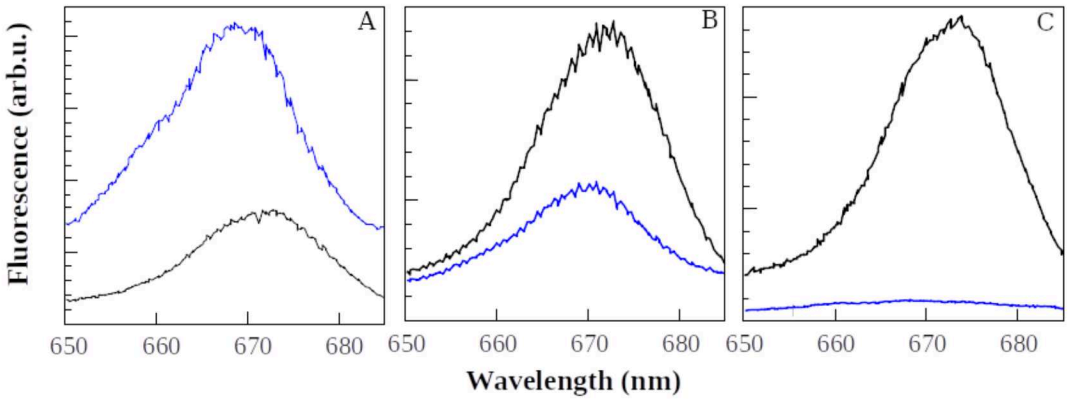

Figure 4.4: Fluorescence excitation spectra for the newest protonated sample (in **A**), the older protonated sample (in **B**), and deuterated sample (in **C**) used in our experiments. The blue curve is for detection at greater than 850 nm, meaning EET occurs from Chls to BChls, and the black curve is for detection between 700 and 750 nm, meaning there is no EET involving the Chls. In **A**, there is a substantial amount of EET-capable Chls, whereas in **B**, there are more EET-incapable Chls. In **C**, there are practically no EET-capable Chls compared to the protonated samples.

4.3 Results

4.3.1 Illumination-intensity Dependence in Modified LH2

Based on interpretations of Förster EET theory, we assumed there would be very poor spectral overlap between BChls and Chls. This would mean there would be limited energy transfer to the BChls. Thus, Chl ZPLs would be narrow and sensitive to temperature. However, it turned out that each sample had varying amounts of EET-capable and EET-incapable Chls (see Figure 4.4) and, therefore a fraction of Chls could actually exchange energy with BChls. These Chls were assumed to be in the so-called proper B800 "pocket" of LH2. Chls which did not transfer energy to BChls were then assumed to be in some "wrong place". Where they ended up is anyone's guess, but there is a lot of evidence that they were not floating around the LH2 in solution given the extensive chromatographic methods described in Section 4.2. Chls that do exchange energy with BChls do it so quickly (around 7 ps) that their holes are broadened. This broadening makes it difficult to observe local heating. As there was evidence that EET-incapable Chls were still attached to the protein (and not just free Chls in solution) we decided to use the EET-incapable

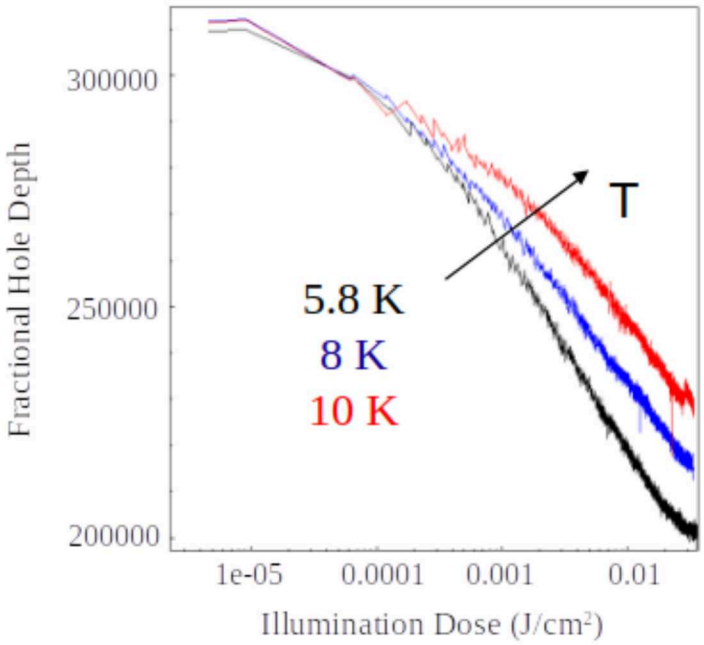

Figure 4.5: HGK curves for our modified LH2 sample. As is seen, with increasing temperatures, hole burning slows down. This means that Chls in our modified LH2 have a temperature dependence and can therefore be used as thermometers.

fraction as thermometers anyway. Holes were burnt at 670 nm in order to examine the temperature dependence of the HGK without BChls, or, simply put, to "calibrate" the Chls as thermometers. The detection window was chosen to be between 700 and 750 nm in order to selectively observe emission from the Chls which do not transfer energy to BChls. Temperature dependence was also observed in the deuterated sample when detection was done in the same wavelength range as shown in Figure 4.5, meaning that the sample could be affected by temperature, confirming the Chls could potentially feel the effects of local heating.

As shown in Figure 4.6, after several attempts at illuminating the BChl around 800 nm in the deuterated sample, nothing came to light, meaning no HGK dependence at 670 nm with illumination at 800 nm. We were never able to observe an intensity-dependence on any HGK, likely because we could not get a high enough intensity light on the BChls. We make this assumption as we used a white light lamp with filters which only allowed light at around 800 nm. Given the full spectral range of the lamp was very wide, this meant only

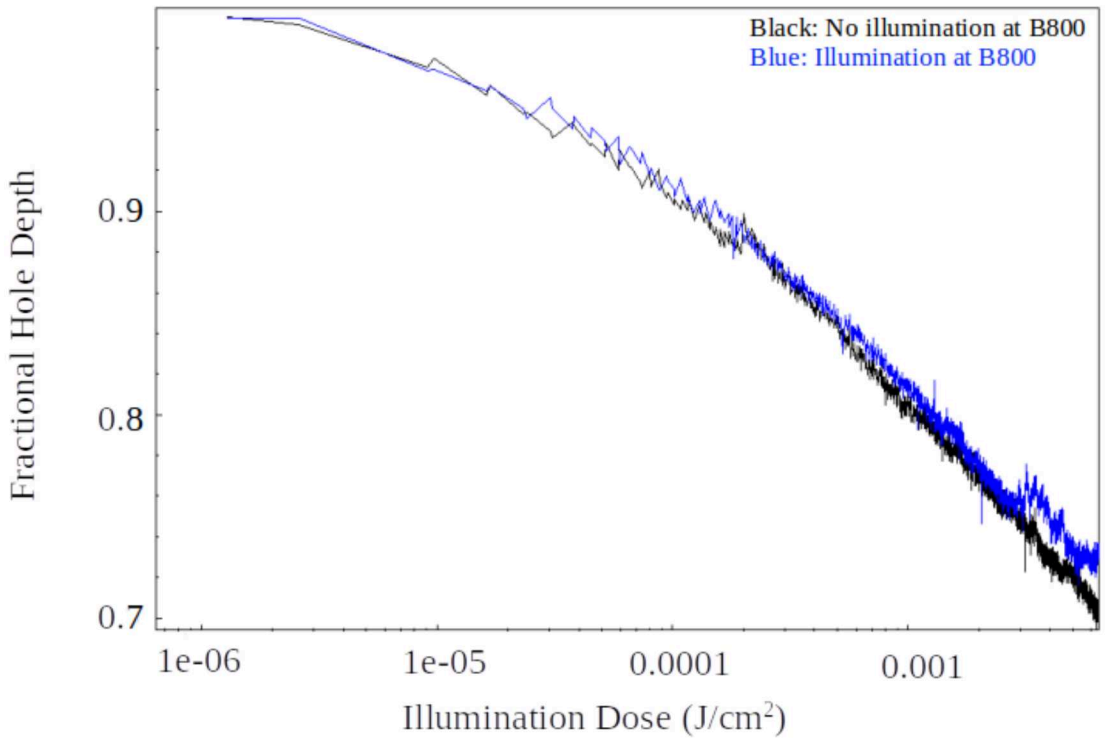

Figure 4.6: Experimental attempts at demonstrating illumination-intensity dependence of the Chls in the deuterated sample of our modified LH2 with a burn wavelength of around 670 nm. In black, B800 BChls were not illuminated. In blue, B800 BChls were illuminated, indicative of local heating. As can be seen, the two curves overall overlap, meaning we were unable to observe an illumination-intensity dependence in our Chls in the modified LH2. There is a step in the blue curve (with illumination at 800 nm), but this is likely a meaningless artifact due to a potential shift of the laser rather than a sudden dependence in illumination.

a small fraction of energy (approximately tens of mW) was contained in a narrow spectral region around 800 nm.

4.3.2 Triplet States

However, we did observe a strong intensity effect on HGK for Chls in modified LH2 in both protonated and deuterated environments, that is, dependence of HGK on the intensity of 670 nm light. This effect was stronger than in cytochrome b_6f. Additionally, it seems our hole growth kinetics and actual hole spectra gave different hole depth values. For instance, as seen in Figure 4.7, in **C** for modified LH2, HGK curves predicted a 41% deep hole, but instead, as shown in **D**, we had a 47% deep hole. Having noticed this discrepancy, we looked

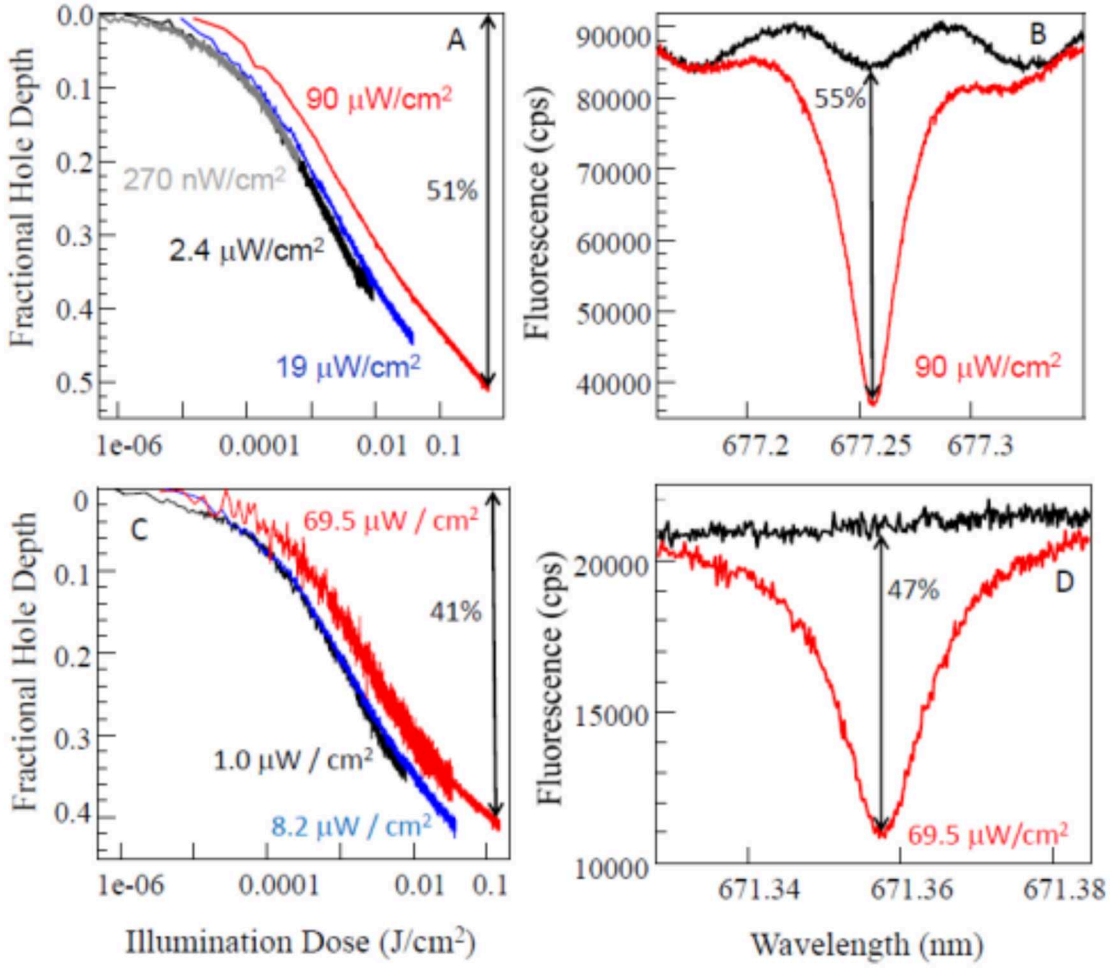

Figure 4.7: In **A**, we see the HGK for cytochrome b_6f (protonated sample shown here) from [Levenberg et al., 2017], with an expected hole depth of 51%. However, in **B**, the immediate post-burn spectrum of cytochrome b_6f indicates the hole was actually burnt to 55%. Similar results were observed in **C** for our modified LH2 (protonated sample shown here) where the hole was expected to be 41%, but, as in **D**, the post-burn spectrum actually shows a hole depth of 47%. While shown for the protonated sample, this same discrepancy was observed for deuterated samples for both complexes. In **A** and **C** we also note that an intensity dependence is present, with increasing intensities leading to slower HGK curves for both samples [Trempe et al., 2021].

at our unpublished cytochrome b_6f data to see if such an effect was also visible. This was confirmed when examining high-enough intensity data: as seen in **A**, we believed (based on HGK) that the hole in our cytochrome b_6f might have grown to 51%. However, the post-burn hole observed was actually 55% as shown in **B**.

The significantly deeper post-burn spectra compared to the expected HGK prediction,

as well as the intensity dependence we observed, could be explained in two ways. The first is by local heating of the protein by several K. It is already known that the homogeneous ZPL width is strongly influenced by temperature, both due to coupling between electronic transitions and small-barrier TLSs and/or local vibrations [Jankowiak et al., 2011] [Najafi et al., 2012] [Najafi et al., 2015]. This leads to a smaller probability of absorption by the ZPL and slows down the HGK with increasing temperature. As previously stated in Section 4.1.1, interface heat conductivity rather than bulk conductivity could potentially be the reason behind seeing an intensity effect in the system.

All the same, clearly we were unable to observe strong local heating effects in our modified LH2 system upon illumination at 800 nm as shown in Figure 4.6. This leads us to the second reason we might observe discrepancies between HGK depths and post-burn spectral hole depths: the presence of triplet states. We shall now go into more detail of this model.

In Section 3.2, the simplest manner (a TLS) of describing a pigment in a protein environment was introduced. In the double-well potential model, there exists both a ground and excited singlet state, each with two wells, shown originally in Figure 3.5 and now in Figure 4.8 **A**. This meant that, when performing NPHB at very low temperatures, the pigment in the first ground state well could become excited into the first excited state well and tunnel through the barrier potential into the second excited state well, before eventually losing energy and going down to the second ground state well. Introducing a triplet state into the model involves a third state the pigment may stay in during NPHB. As shown in Figure 4.8 **B**, using the left wells as an example, there is a third state involved for each well where the pigment may relax to from the excited state and then can further relax back into the ground state. It is well-known that one source of photodamage in plants involves Chl triplet states. Excited Chls can transition to a triplet state and, in aerobic conditions, its energy can then be transferred to molecular oxygen. This leads to a highly oxidizing singlet oxygen and can lead to photoinhibition, meaning the plant's capacity for photosynthesis is reduced [Santabarbara et al., 2007]. In plants, however, photoprotective features, such as funneling triplet energy to carotenoids, can stop the Chl triplet states from being transferred to oxygen [Horton and Ruban, 2004]. While a short-lived triplet

state might not affect our results, if the pigment had the chance to "live" in this triplet state for a long period of time (where long means longer than the few nanseconds), then it would not participate in the NPHB. At room temperature, Chls have been observed to have triplet lifetimes on the order of tens of microseconds [Niedzwiedzki and Blankenship, 2010] [Kosumi et al., 2018], with increasingly longer lifetimes of up to several milliseconds at the much colder 5 K [Suisalu et al., 1980] [Krasnovsky, 1982] [Mauring et al., 1987] [Angerhofer, 1991] [Groot et al., 1995], with potential triplet yields as high as 0.4 [Suisalu et al., 1980]. Broad, shallow, transient holes due to triplet states has been observed in CP43 [Jankowiak et al., 2000] and CP47 [Neupane et al., 2010] [1] core antenna complexes of PS II at a very low 5 K temperature upon non-resonant excitation. The BRC of purple bacteria and RC of PS II have also been observed to have resonant and non-resonant transient holes, although in the RCs, transient holes were due to charge separation [Lyle et al., 1993] [Riley et al., 2004]. Therefore, we know that triplet lifetimes increase with lower temperatures, such as those used in NPHB. As well, in the presence of triplet states, we need to assume transient holes were present, that is, holes that are present, but are only present while the sample is illuminated. The transient hole would imply that molecules were in that triplet state and they were unavailable to contribute to absorption and to persistent hole. Therefore, there would be a slowdown of the hole burning since the pigment is clearly unavailable to partake in the process, which would lead to saturation broadening of the ZPL. This matches up quite well with the results we observed for our modified LH2 and cytochrome b_6f: our HGK indicated a much smaller hole (slowdown) than our post-burn hole showed.

Most papers which detailed the effects of triplet states on SHB focused on spectral diffusion, without fully explaining the discrepancies we had observed [Vries and Wiersma, 1980] [Müller et al., 1998]. For example, while [Müller et al., 1998] did model some HGK, as well as provide easy-to-use expressions for ZPL broadening profiles and SDF modified due to transient holes, some variables were overlooked. For example, it seems they ignored a key point that, within the first triplet lifetime of hole burning, dynamic equilibrium is set for the populations of the three states, and that resonant absorption is reduced before the

[1] Both CP43 and CP47 are transmembrane proteins found in PS II.

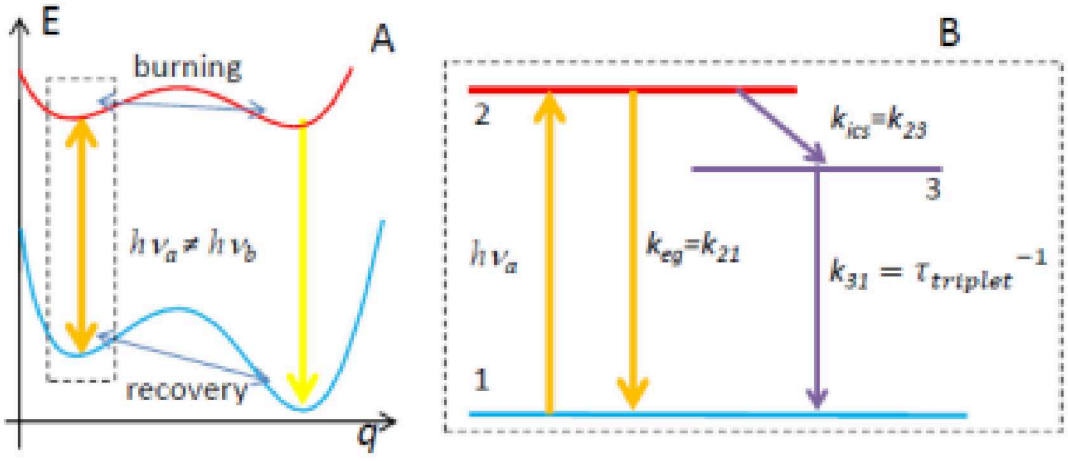

Figure 4.8: In **A**, we have the previously introduced TLS, with the blue curve showing the ground singlet state and the red curve showing the excited singlet state. Using the first wells as an example, zooming in on the dashed box in **B**, we see that rather than the pigment occupying only two possible states, it may also occupy another third state, shown in purple [Trempe et al., 2021].

first data point of the HGK is even collected. In [Vries and Wiersma, 1980], a detailed theory was introduced, based on a density matrix approach, that explained either purely transient holes (where the probe beam is weak/non-saturating), or persistent hole shapes after burning with an intense beam had ended. Thus, it didn't cover the situation of HGK measurements where the probe beam is the exact same beam causing triplet-related saturation broadening. Finally, neither [Müller et al., 1998] nor [Vries and Wiersma, 1980] included a distribution of α angles between the transition dipole $\boldsymbol{\mu}$ and electric field $\boldsymbol{E}$. Thus, in order to test if triplet states were the source of the mismatching, HGK simulations were done taking into account the effects mentioned. Here we re-state the NPHB equation seen in Eq. 3.3.2

$$D(\Omega,t) = \frac{3}{2}\int d\omega L(\Omega-\omega)G(\omega)\int d\lambda f(\lambda)\int d\alpha \sin\alpha\cos^2\alpha e^{-P\sigma\phi(\lambda,\tau_{fl})L(\omega_B-\omega)t\cos^2\alpha} \tag{4.3.1}$$

and describing the variables to accommodate the presence of triplet states. To ensure it is clear, we will describe the variables affected by triplet states here:

1. $L(\omega)$ which is the single site spectrum (SSS) shape. It contains information on the ZPL

and PSB [Reinot and Small, 2000]. This means if the ZPL were saturation-broadened because of the triplet state, the SSS shape would obviously change.

2. α which is the angle between the electric field of the light and the transition dipole moment vector of the chromophore. Here, the distribution of α explicitly spelled out in the NPHB master equation represents the random isotropic orientation of the chromophores. Previously, the effects of this distribution were found via an approximation formula. In the case where triplet states are present, if $\boldsymbol{E}$ and transition dipole $\boldsymbol{\mu}$ are parallel, the ZPL is maximally saturation broadened. If they are perpendicular, it is not. Consequently, we had to consider the dependence of saturation broadening on α, and, given the failure of the approximate formula, we did real numerical integration over α.

3. $G(\omega)$ is the site distribution function (SDF). This was modified depending on the α chosen given that, depending on $\boldsymbol{E}$, $\boldsymbol{\mu}$, and P, the SDF would be correspondingly modified by a transient hole emerging in the first few milliseconds of burning.

4. Finally, for ϕ, which is the NPHB yield, that is, the probibility of NPHB, we end up with the following equation:

$$\phi(\lambda) = \frac{\Omega_0 exp(-2\lambda)}{\Omega_0 exp(-2\lambda) + k_{ics} + \tau_{fl}^{-1}} \tag{4.3.2}$$

where k_{ics} is the intersystem crossing rate. In the original NPHB yield equation, Eq. 3.3.1, this term was absent. However, now that we have a triplet state, the pigment has the opportunity to go to this state and an intersystem crossing rate factor needs to be noted, as seen in Figure 4.8.

With this short explanation, we can now briefly summarise the equations from [Vries and Wiersma, 1980] [Müller et al., 1998] and further expand on them, which allowed us to complete our modelling.

First, after applying the rotating wave approximation, [Vries and Wiersma, 1980] provides the set of equations of motion for the relevant density matrix elements

$$\dot{\rho}_{11} = k_{21}\rho_{22} + k_{31}\rho_{33} + \frac{1}{2}i\chi(\overline{\rho_{21}} - \overline{\rho_{12}}) \tag{4.3.3}$$

$$\dot{\rho}_{22} = -k_{21}\rho_{22} - k_{23}\rho_{22} + \frac{1}{2}i\chi(\overline{\rho_{12}} - \overline{\rho_{21}}) \tag{4.3.4}$$

$$\dot{\overline{\rho_{12}}} = (i\Delta - \frac{1}{T_2})\overline{\rho_{12}} + \frac{1}{2}i\chi(\rho_{22} - \rho_{11}) \tag{4.3.5}$$

$$\dot{\rho_{12}} = k_{23}\rho_{22} - k_{31}\rho_{33} \tag{4.3.6}$$

$$\rho_{11} + \rho_{22} + \rho_{33} = 1 \tag{4.3.7}$$

Subscript 1 refers to the singlet ground state (blue state in Figure 4.8), subscript 2 refers to the singlet excited state (red state in Figure 4.8), and subscript 3 refers to the triplet state (purple state in Figure 4.8). $\chi = \mu E cos(\alpha)/\ \hbar$. T_2 determines the homogeneous line width Γ_{hom}, where the line width affects the peak absorption cross-section ϵ_0; it is affected by $2 \rightarrow 1$ processes and by pure dephasing. $\Delta = \omega_B - \omega$ is detuning with respect to the ω_B, the burn frequency, which is resonant with the $1 \rightarrow 2$ transitions. $k_{23} = k_{ics}$ is the intersystem crossing rate, $k_{21} = k_{eg} = {\tau_1}^{-1}$ and $k_{31} = {\tau_{triplet}}^{-1}$.

From Eq. 4.3.3 to Eq. 4.3.7, the steady-state population difference between the ground singlet state and the excited singlet state are defined as (Eq. 18 from [Vries and Wiersma, 1980])

$$\rho_{11} - \rho_{22} = \frac{\Delta^2 + \frac{1}{T^2}}{\Delta^2 + \frac{1}{T^2} + K^2} \tag{4.3.8}$$

where $K^2 = \frac{\chi^2(2+A)}{2T_2(k_{21}+k_{23})}$ and $A = \frac{k_{23}}{k_{31}} = k_{ics}\tau_{triplet}$. It is important to note that K^2 is proportional to E^2, that is, proportional to photon flux P and to $cos^2\alpha$. As well, Eq. 4.3.8 describes one minus a flux-dependent Lorentzian. This is the function which is multiplied by the pre-burn SDF (or $G(\omega)$ in Eq. 4.3.1) to obtain the SDF containing the transient hole.

Without illumination for any Δ, $\rho_{11} - \rho_{22} = 1$, $\rho_{11} = 1$, $\rho_{22} = 0$, and $\rho_{33} = 0$. With zero detuning ($\Delta = 0$) at ω_B and with very large photon flux, $\rho_{11} - \rho_{22} \rightarrow 0$.

The fraction of the SDF which remains at ω_B after the transient hole is formed (Eq. 4.3.8 with zero detuning) gives

$$\frac{\frac{1}{{T_2}^2}}{\frac{1}{T_2}^2 + K^2} = \frac{1}{1 + K^2T^2} = \frac{1}{1 + \frac{P\cos^2\alpha}{P_s}} \tag{4.3.9}$$

where P_s is the saturation photon flux, a quantity more compatible with our master equation Eq. 3.3.2 and Eq. 4.3.1 and deviating from [Müller et al., 1998] as it now contains explicit angular dependence. The saturation photon flux is defined by

$$P_s = \frac{k_{31}(k_{21} + k_{23})}{(2k_{31} + k_{23})\epsilon_0} \approx \frac{k_{31}(k_{21} + k_{23})}{k_{23}\epsilon_0} = \frac{1}{\tau_{triplet}\theta\epsilon_0} \tag{4.3.10}$$

where, as long as the triplet lifetime is much longer (that is, milliseconds-long) than the singlet excited state lifetime (in nanoseconds), then we can assume $k_{31} << k_{23}$. We define $\theta = \frac{k_{ics}}{(k_{eg}+k_{ics})} = \frac{k_{23}}{(k_{21}+k_{23})}$ as the intersystem crossing yield. ϵ_0 is the peak absorption cross-section of the unsaturated ZPL defined as $\epsilon_0 = \sigma L(\omega_{ZPL})$. It should be noted that the full single-site spectrum (SSS) (which contains the non-broadened ZPL, PSB, and intramolecular vibrations) was used to obtain ϵ_0 from the integral cross-section σ (which is determined in the absence of saturation).

If the remaining SDF at ω_B is defined by Eq. 4.3.9, then the fractional depth of the transient hole in the SDf is defined as

$$\frac{\Delta G(\omega_B)}{G(\omega_B, P = 0)} = 1 - \frac{1}{(1 + \frac{P\cos^2\alpha}{P_s})} = \frac{(\frac{P\cos^2\alpha}{P_s})}{(1 + \frac{P\cos^2\alpha}{P_s})} \tag{4.3.11}$$

For low flux P or perpendicular $\boldsymbol{E}$ and $\boldsymbol{\mu}$, this fractional depth $\to 0$. For large flux P and parallel $\boldsymbol{E}$ and $\boldsymbol{\mu}$, this quantity $\to 1$. In [Müller et al., 1998], the saturation-broadened Lorentzian ZPL was written as

$$L(\Delta, a, P) = \frac{\epsilon_0{\Gamma_{hom}}^2}{\Delta^2 + (1 + \frac{P\cos^2\alpha}{P_s}){\Gamma_{hom}}^2} \tag{4.3.12}$$

however, without the angular dependence. In the case of zero phonon flux (that is, $P = 0$), the peak of this line is normalised to $\epsilon_0 = \sigma L(\omega_{ZPL})$. From Eq. 4.3.12, it's seen that the saturation-broadened, single-molecule ZPL has a width of $\Gamma_{hom} = \sqrt{1 + \frac{P\cos^2\alpha}{P_s}}$ and the peak is reduced by a factor of $1 + \frac{P\cos^2\alpha}{P_s}$.

In order for us to obtain accurate simulations, the α distribution was not approximated,

as was done in [Reinot and Small, 2000] and previously mentioned, but instead, specific values were used. With a step of five degrees between 0 and 90 degrees, first, a purely transient hole in the SDF was considered. This was the result of the dynamic equilibrium established within a several-millisecond-long $\tau_{triplet}$, which is much a smaller time interval than one datapoint of our experimentally-measured HGK curves (where the duration ranges from 50 to 500 ms). The small amount of persistent hole burning which occurs in the first $\tau_{triplet}$ of illumination was ignored. This transient hole was used to pre-modify the $G(\omega)$ used for subsequent persistent holes. This meant we accounted for the chromophores which were unavailable to contribute to the NPHB as they were in the triplet state for resonant excitation. We also assumed the transient hole in the SDF was purely Lorentzian. This could be assumed based on the fact that, for narrow ZPL where there is no EET or charge separation on the single-ps timescale as well as small-to-moderate electron-phonon coupling, the peak absorption cross-section for the PSB is two orders of magnitude smaller than for the ZPL. Illumination of the PSB is unlikely to cause saturation effects. Simply put, there is no transient pseudo-PSBH for a narrow, transient ZPH.

For modelling of our HGK curves, for every α we used two different SSS where one had the saturation-broadened ZPL and the other had a non-broadened ZPL. Broadened-ZPL SSS with a reduced peak absorption cross-section was used in the exponential term of Eq. 3.3.2 and Eq. 4.3.1, the NPHB master equation. The modified SDF was convoluted with non-broadened SSS in order to get a spectral hole shape assuming a weak (non-saturating) probe beam was used. This corresponds to the situation shown in Figure 4.7 in **B** and **D**, as well as in [Müller et al., 1998], where the post-burn hole spectra were measured with low power after the hole was burnt. The SDF which were modified by both transient and persistent holes were convoluted with SSS containing the saturation-broadened ZPL in order to obtain the hole shape during HGK measurements. In essence, Eq. 3.3.2 and Eq. 4.3.1 were transformed into

$$D(\Omega,t) = \int d\omega \int d\lambda f(\lambda) \int d\alpha L'(\Omega-\omega,\alpha,P)G(\omega)[\rho_{11}-\rho_{22}](\omega_B-\omega,\alpha,P) \\ \frac{3}{2}\sin\alpha\cos^2\alpha e^{-P\sigma\phi(\lambda)L_B(\omega_B-\omega,\alpha,P)t\cos^2\alpha} \quad (4.3.13)$$

where $[\rho_{11} - \rho_{22}](\omega_b - \omega, \alpha, P)$, the SDF modification by transient hole, is described in Eq. 4.3.8; $L_B(\omega_b - \omega, \alpha, P)$ is the SSS which contains the broadened ZPL, PSB, and intramolecular vibrations; and $L'(\Omega - \omega, \alpha, P)$ is the SSS with broadened ZPL for HGK or non-broadened ZPL for spectral holes measured with weak probe beams. The integral of $L_B(\omega_b - \omega, \alpha, P)$ was no longer normalised to one, which can be reasoned to be because of a reduction of the integral absorption cross-section when saturated. We also remind you that the NHPB yield is now defined by Eq. 4.3.2, which contains a k_{ics} term.

Producing one set of HGK curves and post-burn hole spectra took several hours on an i7 computer with 32 GB of RAM. Figure 4.9 shows the results of these simulations. First, holes were modelled with the modified NPHB master equation Eq. 4.3.13 at three different, increasing intensities: 19 μW/cm^2, 90 μW/cm^2, and 270 μW/cm^2. The intersystem crossing yield was $\theta = 0.2$ and the triplet lifetime was $\tau_{triplet} = 2.0ms$.

For any dose, the depth of the purely transient component of the hole in the SDF is roughly the same percentage of the remaining SDF at ω_B, with this percentage increasing with intensity. The absolute magnitude of the purely transient part decreases with dose as there is less and less SDF remaining at ω_B. In order to obtain the purely-persistent-hole curve, which reflects the evolution of the observable persistent holes, the purely persistent component of the hole in the SDF is convoluted with the SSS containing narrow, non-saturated ZPL. And to obtain the transient-and-persistent curve in Figure 4.9, the hole in the SDF is convoluted with the SSS containing saturation-broadened ZPL with reduced peak intensity. Consequently, the blue and black curves in Figure 4.9 in **B** and **C** may eventually intersect. Since in actual experiments knowledge of the presence and depth of a transient hole is absent, this persistent-and-transient black curve was normalized to start at 0 depth as in experimental Figure 4.9 **A** to **C** and presented in red. At low intensities, such as in **A** at an intensity of 19 μW/cm^2, transient holes, and therefore the presence of a triple state, did not influence the hole growth significantly. However, as intensities increase, the hole burning clearly slows down with that transient component, as shown through the red curves and blue curves in **B** and **C**. And, in fact, this matches up quite well with the 4-6% difference we saw between HGK curves and post-burn holes in Figure 4.7 where an intensity of 70-90 μW/cm^2 was used experimentally. We were able to simulate very similar

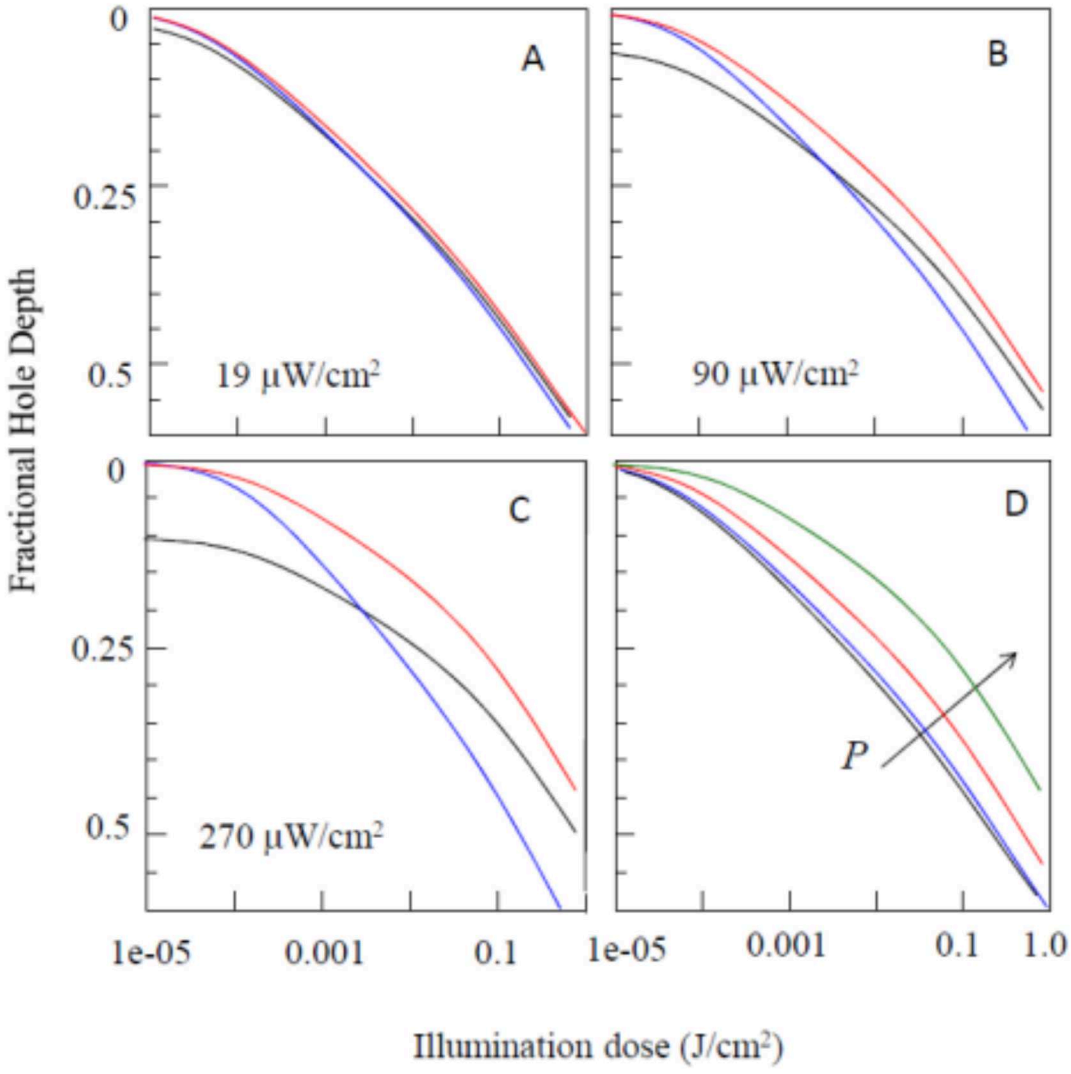

Figure 4.9: Through the use of the SHB master equation, in **A** to **C**, HGK curves were calculated for 19, 90 and 270 μW/cm^2 respectively. $\tau_{\text{triplet}} = 2.0$ ms, $\theta = 0.2$. The blue curve contains strictly persistent holes. The black curve contains both persistent and transient holes. The red curve is the black curve re-normalised to start at 0 given that it is impossible to know the presence of a transient hole (if there is any) prior to HGK. As one can see, with increased intensities, the presence of a transient hole and a triplet state grows in importance and shows a slowdown in the HGK. In **D**, the curves contain both transient and persistent components re-normalized to start at zero (i..e red curves from Frames **A** to **C**). Black, blue, red, and green curves are for 4.3, 19, 90 and 270 μW/cm^2, respectively. Again, one can note that with increasing intensity, the hole growth rate decreases, indicating that triplet states can become visible at higher intensities [Trempe et al., 2021].

results with an intensity of 90 μW/cm^2, a triplet lifetime of $\tau_{triplet} = 2.0$ ms, triplet yield of $\theta = 0.2$, and an integral absorption cross-section of 4.3×10^{-13} cm^2 cm^{-1} as presented in **B**. At increasingly higher intensities as in **C** at 270 μW/cm^2, the hole continues to grow even more slowly. It should be noted that the transient holes only showed a small depth (the black curves in **A** to **C**) due to the α-distribution. In fact, the fractional depths of transient holes when the electric field and the transition dipole were parallel were much larger. In Figure 4.9 **D**, the accumulated red curves from **A** to **C** were placed together to show the intensity dependence of HGK.

The following parameters were assumed in order to obtain the curves in Figure 4.9: $\Gamma_{hom} = 0.0256\text{cm}^{-1}$, $\tau_1 = 3.125$ns, the electron-phonon coupling $S = 0.72$ (along with other electron-phonon coupling parameters of OGP-solubilised cytochrome b_6f [Najafi et al., 2015] [Levenberg et al., 2017] [Shafiei et al., 2019]), and the distribution of the tunnelling parameter λ was uniform between 7.8 and 13.1 with $\Omega_0 = 7.6 \times 10^{12} s^{-1}$. Changing the τ_1 allowed us to keep the effective singlet excited state lifetime (which is now affected by k_{eg} and k_{ics}) at 2.5 ns [Levenberg et al., 2017] [Shafiei et al., 2019] with $\theta = 0.2$ and therefore, to keep the NPHB yields the same for λ values used previous papers published by our research group.

Before moving on, it should be noted that the integral absorption cross-section we mentioned above, presented in Eq. 4.3.13, was an assumed value. We will briefly explain here how it was estimated.

First, we used the room temperature spectrum of Chl *a* in diethyl ether (with molar extinction coefficient of 85 000 M cm^{-1} at the peak of the Q_y band measured in solution using a spectrometer with a non-polarised beam, and corresponding peak absorption cross-section of 3.5×10^{-16} cm^2) [Du et al., 1998]. The peak absorption cross-section measured when the electric field $\boldsymbol{E}$ and transition dipole $\boldsymbol{\mu}$ are parallel is larger at 1.05×10^{-15} cm^2. The full-width at half-maximum (FWHM) of the Chl *a* band was found to be 390 cm^{-1} at room temperature. However, the FWHM is affected by homogeneous and inhomogeneous broadening and by 120 K, the Q_y absorption of Chl *a* in the organic solvent narrows to about 290 cm^{-1} mostly due to inhomogeneous broadening [Rätsep et al., 2009]. If we assume that, at room temperature, both the homogeneously-broadened line and the SDF

are Gaussian, and we also assume that the inhomgeneous line FWHM is about 280 cm^{-1}, then the room temperature homogeneous line FWHM should be about 270 cm cm^{-1} and the integral absorption cross-section σ should be about $4.3 \pm 0.3 \times 10^{-13}$ cm^2 cm^{-1}. If we convolute two very-similarly-wide Gaussians, this produces a Gaussian with an increased width of about $\sqrt{2}$ and a decreased peak by about $\sqrt{2}$. The peak of the homogeneously-broadened line convoluted with the SDF normalised to one must be $\sqrt{2}$ higher than the peak of the resulting absorption band. Finally, the area under a Gaussian with a FWHM of 270 cm^{-1} and a peak amplitude of one gives 290.

Now we will examine how triplet lifetimes were simulated in a deuterated environment. Triplet lifetimes depend on solvent. Previous research showed that, when placed in deuterated ethanol, triplet lifetimes for Chl *a* can increase by around 25% compared to regular ethanol [Mauring et al., 1987] [Angerhofer, 1991]. The triplet lifetime of sulphonated aluminum phthalocyanine in a deuterated aqueous solvent can increase by a factor of nearly three [Beeby et al., 1992]. It was assumed that deuteration would result in a decrease of the $P_s = \frac{(\tau_{triplet})^{-1}}{\theta\epsilon_0}$, mostly due to the increase of the triplet lifetime.

As shown in Figure 4.10, we ran the simulations at 19 $\mu W/cm^2$ with varying triplet lifetimes of 1 ms to 5 ms for cytochrome b_6f in **A**, and at 90 $\mu W/cm^2$ for those same varying triplet lifetimes for modified LH2 in **B**. That means simulations were run with the largest intensity for which we have data on cytochrome b_6f and modified LH2 in both protonated and deuterated environments. Sometimes higher-intensity data was available only from one sample or another, but not both. In **A** for cytochrome b_6f, we clearly see a slowdown of the HGK with these longer triplet lifetimes. However, when compared to the cytochrome b_6f experimental results in the insert, the difference between 1.0 ms and the 5.0 ms curves (so a factor of five difference in the triplet lifetime) is still smaller than the difference we saw experimentally. In **B**, the intensity simulated for modified LH2 was somewhat above what we used experimentally (69.5 $\mu W/cm^2$). As well, before renormalising, about a 3% fractional hole depth of the transient hole was observed for a triplet lifetime of 1.0 ms and about a 10% increase for $\tau_{triplet}$ = 5.0 ms. As can be noted with the insert, again, the five-fold increase in the triplet lifetime only begins to match the deuteration effect we noticed experimentally for modified LH2. Consequently, while we can certainly say triplet

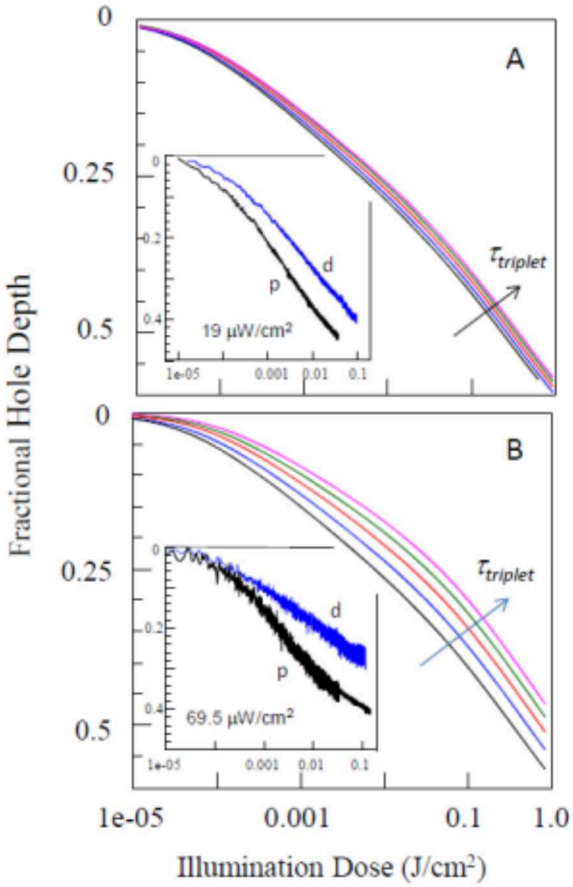

Figure 4.10: In **A**, simulated HGK curves for cytochrome b_6f re-normalised to begin at 0 depth, performed at 19 μW/cm^2. Black, red, blue, green and magenta curves are for τ_{triplet} = 1.0, 2.0, 3.0, 4.0 and 5.0 ms, respectively. The insert showing both the deuterated (d) and protonated (p) experimental results for the complex. In **B**, simulated HGK curves for modified LH2, re-normalised to start at 0, and performed at 90 μW/cm^2. Coloured curves correspond to the same triplet lifetimes as **A**. In this case, the insert shows HGK of Chl *a* in the modified LH2 at an intensity of 69.5 μW/cm^2. As one can note, even at a five-fold increase of τ_{triplet} in the simulations, it isn't enough to describe the deuteration effect noted experimentally [Trempe et al., 2021].

lifetimes had an effect on HGK, the deuteration effect is too strong to be explained by it alone. Therefore, local heating could still be considered part of the explanation.

4.3.2.1 Discussion

We know that Chl *a* triplet-state parameters are temperature dependent. That is, triplet lifetimes have been reported to be on the order of tens of microseconds at room temperature for a pigment placed in an organic solvent [Niedzwiedzki and Blankenship, 2010]

[Kosumi et al., 2018]. The lifetimes also depend on, for example, the solvent used, the Mg coordination number (that is, how many atoms/molecules are bound to that central Mg atom in the Chl *a* molecule), the presence of triplet quenchers in the solution, as well as other factors. As we had mentioned previously, Chl triplet lifetimes increase with decreased temperatures, with several milliseconds reported at 5 K and triplet yields as high as 0.4. In core complexes [Zabelin et al., 2016] and reaction centres of PS II [Neverov et al., 2015], triplet lifetimes of 1.5-1.6 ms were reported. As for the CP47 antenna complex at cryogenic temperatures, bi-exponential kinetics with lifetimes of 0.6 and 2.0 ms with triplet yields of 0.16 were reported [Groot et al., 1995]. Consequently, our assumption that the average triplet lifetime was 2.0 ms and the intersystem crossing yield $\theta = 0.2$ should be reasonably accurate. In our simulations, we did not attempt to perfectly fit our curves to experimental data by manipulating different triplet parameters. Nonetheless, we feel confident enough to say that our ϵ_0 (peak absorption cross-section of the unsaturated ZPL), $\tau_{triplet}$, and θ (intersystem cross yield) are correct within a factor of two. We should note that our ZPLs at 5 K are narrower than 1 GHz for the lowest energy states of the antenna proteins (as well as for cytochrome b_6f or Chl *a* not transferring energy to BChl *a* in modified LH2 in our case), though inhomogeneous Q_y bandwidths of Chl *a* are on the order of several thousand GHz. As shown in Figure 4.9 **B**, approximately 7% transient holes are expected for resonant excitation with around 100 μW/cm^2. Non-resonant excitation with an intensity three orders of magnitude higher (that is, around 100 mW/cm^2) would result in broad, non-resonant, transient holes with depths of around 1%. For cytochrome b_6f, we verified that with illumination at 445 nm with about 500 mW/cm^2 at 77 K would result in about a 2% transient bleach of the Chl *a* Q_y band. Consequently, observations of deeper transient bleaches in the antenna proteins due to "triplet bottleneck" effects [Jankowiak et al., 2000] [Neupane et al., 2010] most likely require longer than average triplet lifetimes and/or higher triplet yields.

As shown in Figure 4.9 **D**, when our hole burning model incorporates Chl triplet states with a lifetime in the millisecond range, there is a very clear and significant intensity dependence of the HGK. As well, as shown in Figure 4.9 **B** and **C**, there are obvious discrepancies between the hole depths obtained from HGK (red curve) and those observed

after higher-intensity burning by tuning a weaker probe beam (blue curve). This is important to keep in mind when fitting HGK data to obtain the distribution of the tunnelling parameter in the excited state. This is also particularly important when using high-intensity HGK while ignoring triplet-related effects as this means you are trying to fit the experimental data to the blue-type curve in Figure 4.9 **A** to **C** when it should, in fact, be fitted to the red-type curve. This misinterpreted fit would lead to an overestimation of the mean and width of our λ distribution. For example, let us assume that the experimental data was represented by the red HGK curve for 90 μW/cm^2 in Figure 4.9 **B**. Normally, the uncertainties of the parameters of the λ distribution obtained from the fits to experimental data are less than 0.1. We could easily fit the curve without triplets and using a uniform λ distribution with $\lambda_{min} = 8.3$ and $\lambda_{max} = 13.8$. However, with triplets present, the values are $\lambda_{min} = 7.8$ and $\lambda_{max} = 13.1$, and therefore, significantly smaller than without triplets present. To put this into perspective, this is equivalent to reducing the average NPHB yield by a factor of around 3.3. Of course, as stated already, the singlet excited lifetime of 2.5 ns was used when there was no triplet to keep the same NPHB yield for the same tunnelling parameter. All that to say, invoking triplet states allows for a smaller λ to be used to fit the same experimental data and, as stated in a previous paper from our research group [Najafi et al., 2015], using a smaller λ allows us to get better quantitative agreement between simulations and experiments, including HGK, fixed-temperature recovery, and thermocycling. See Table 4.1 for the different parameters used for Figure 4.9 **B**.

As already noted, solvent deuteration can increase the triplet lifetime of Chl *a* to a degree (by 25% for deuterated ethanol). Sulphonated aluminum phtalocyanine placed in a deuterated acqueous solvent, in a more extreme case, saw an increased triplet lifetime from 0.6 ms to 1.6 ms, with a triplet yield increasing from 0.40 to 0.52 [Beeby et al., 1992] (which corresponds to a decrease of the saturation flux P_s by a factor of 3.5). Nonetheless, the changes in our simulated curves related to a decreasing of P_s by a factor of 5 still is not large enough to match what we observed in cytochrome b_6f and our modified LH2, seen in Figure 4.10. In [Mauring et al., 1987] and [Beeby et al., 1992], both the Chl *a* and sulphonated aluminum phtalocyanine were in direct contact with the deuterated solvent. Exposure to the water/glycerol mixture can cause effects in Chl *a* in solution

Parameter	**No Triplet**	**With Triplet where $\tau_{triplet} = 2ms$, $\theta = 0.2$**
Non-saturated SSS shape	$\Gamma_{hom} = 0.0256cm^1$, $S_{el-ph} = 0.72$, see [Levenberg et al., 2017]	non-saturated $\Gamma_{hom} = 0.0256cm^1$, $S_{el-ph} = 0.72$, see [Levenberg et al., 2017]
τ_{eg}	2.5 ns	3.125 ns
$\phi(\lambda = 10, \Omega_0 = 7.6 \times 10^{12}s^{-1})$	3.92×10^{-5}	3.92×10^{-5}
λ-distribution	Uniform, 8.3 to 13.8	Uniform, 7.8 to 13.1
Average ϕ	4.8×10^{-6}	1.6×10^{-5}

Table 4.1: A summary of the modelling parameters employed for Figure 4.9 **B** with an intensity of 90 mW/cm^2.

that we did not observe, such as aggregation, strong fluorescence quenching, and very poor persistent hole burning, even when Chls appear monomeric and emit at around 680 nm [Levenberg et al., 2017]. When HGK used low enough burn intensities (less than 10 μW/cm^2), hole recovery dynamics did not show a deuteration effect, which was indicative that the masses of entities involved in tunnelling did not change by more than several percent [Levenberg et al., 2017]. Fluorescence Line Narrowing [2] difference spectra revealed that there was slow energy transfer between two Chl *a* molecules in cytochrome b_6f dimer showing that the cytochrome b_6f was intact and the Chls were not floating in the solvent [Najafi et al., 2015]. In short, triplet states cannot fully explain the strong deuteration effect we saw in our experiments. Thus, local heating is likely still a contributing factor [Levenberg et al., 2017].

Finally, we note that the assumption that transient holes do not contain pseudo-PSBH contributions may not be valid when the ZPLs are broad, when ZPL and PSB peak absorption cross-sections are comparable, and when very high excitation intensities (hundreds of mW/cm^2) are used. For practical purposes, our software is capable of including the full single-site spectrum in transient hole simulations instead of a Lorentzian.

[2] Fluorescence line narrowing is a site-selective spectral technique which uncovers the optical spectra of hidden molecules in an amorphous solid [Fidy et al., 1998].

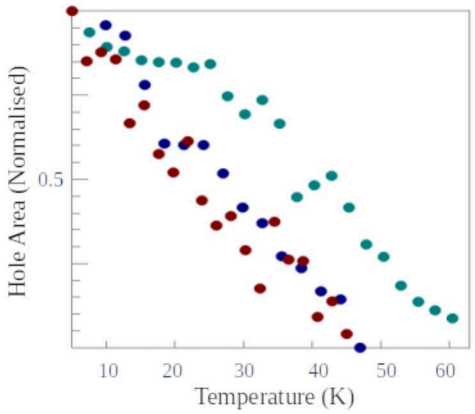

Figure 4.11: Thermocycling recovery results of BChls in regular LH2 (in green), EET-incapable Chls in modified LH2 (in red), and EET-capable Chls in modified LH2 (in blue). Interestingly, BChls in regular LH2 clearly take longer to recover, but thermocycling recovery is similar in modified LH2 regardless of the EET capabilities of the Chls.

4.3.3 Thermocycling Experiments with Modified LH2

A detailed NPHB study of LH2 focusing on energy landscapes rather than triplets is so far unfinished. Still, we present here a brief overview of data from thermocycling-induced recovery experiments. We examined the thermocycling recovery of BChls in regular LH2 and compared it to the thermocycling-induced recovery of both the EET-capable Chls (emission detected at >850 nm) and the EET-incapable Chls (emission detected 700-750 nm), replacing the B800 BChls in LH2. The results are presented in Figure 4.11.

Normally, using our TLS model, we assume that the ground and excited states themselves belong to the Chl, whereas the double-well potential belongs to the protein environment, in this case, LH2. If EET-capable and EET-incapable Chls are in different environments in the protein (which was the expectation), their spectral holes should be recovering differently from each other. On the other hand, given that EET-capable Chls were assumed to be in the same environment as B800 BChls, then spectral holes for EET-capable Chls and B800 BChls should recover similarly. Consequently, we wouldn't expect to see a trend where, in Figure 4.11, the holes for the EET-capable and EET-incapable Chls both recover similarly to each other and significantly faster compared to the BChls. Given that they instead recover similarly, it's possible that the pigment itself contributes to the generalised coordinate in the double-well potential explaining the NPHB.

Chapter 5

Conclusions and Future Work

Several attempts were made to illuminate B800 BChls in modified LH2 placed in a deuterated solvent in order to show that local heating was the reason for a slowdown in HGK curves in cytochrome b_6f. While we were unable to show this relation, this nonetheless led to another observation: that of discrepancies between expected HGK hole depths and actual hole depths, both in protonated and deuterated samples of modified LH2 and cytochrome b_6f. Through modelling, we were able to show that transient holes from triplet states would lead to slower HGK curves with increased intensities. We also showed that increased triplet lifetimes, which would somewhat increase in deuterated solutions, could partially explain the deuteration effect, but it is not the whole story. That is, likely local heating along with triplet states are contributing to the deuteration effect. We also noticed that, when examining thermocycling data of our modified LH2, hole recovery was similar for both EET-capable and EET-incapable Chls, but different for BChls. These considerations have led us to believe that perhaps the pigment itself contributes to the generalised coordinate of a two-level system.

It would be necessary to re-attempt our illumination-intensity experiments with a stronger light source given the possibility that a filtered white lamp was not strong enough to provide enough energy per unit time to be dissipated in B800-B850 transitions. To this end, we have already purchased a 1 W LED, with an emission spectrum matching the shape of the B800 band. If 800 nm illumination did affect HGK in deuterated-solvent LH2 samples, it would also be necessary to perform illumination-intensity dependence experiments of

modified LH2 in a protonated solvent to see if we notice any effects. Furthermore, we could also try exploring these effects in some other complexes, such as CP43, which has relatively deep, non-resonant triplet bottleneck holes.

Given the current construction of a closed-cycle cryostat underway in the lab, it would also be possible to attempt fixed-temperature, week-long, complete-recovery experiments. Normally experiments were only performed for one day given the shortcomings of liquid helium used in the equipment: helium is expensive, refilling the cryostat with liquid Helium results in shaking of the cryostat, and baseline drift occur as all parts hang from the top of liquid helium cryostat. However, with this new cryostat, week-long fixed-temperature hole recovery experiments would be feasible.

As also noted, thermocycling experimentation on parts of modified LH2 are still in their infancy. That is, while we have some potential conclusions on the subject matter, more experiments are necessary to see if and how much the pigment could be affecting the generalised coordinate. Results of thermocycling experiments will be compared with those of fixed temperature recovery, in order to determine the md^2 parameter and gain information on entities involved in tunneling/NPHB in LH2.

References

[Aegon, 2006] Aegon (2006). Image of absorption spectra of bacteriochlorophyll a and lh2 antenna complex, retrieved from https://upload.wikimedia.org/wikipedia/commons/4/4c/lh2_bch_absorption.png (accessed may 4, 2021).

[Alia et al., 2001] Alia, J. M., Soede-Huijbregts, C., Baldus, M., Raap, J., Lugtenburg, J., Gast, P., van Gorkom, H. J., Hoff, A. J., and de Groot, H. J. M. (2001). Ultrahigh field mas nmr dipolar correlation spectroscopy of the histidine residues in light-harvesting complex ii from photosynthetic bacteria reveals partial internal charge transfer in the b850/his complex. *J. Am. Chem. Soc*, 123:4803–4809.

[Anderson et al., 1972] Anderson, P. W., Halperin, B. I., and Varma, C. M. (1972). Anomalous low-temperature thermal properties of glasses and spin glasses. In *Structure and Properties of Condensed Matter*, volume 25 of *The Philosophical Magazine: A Journal of Theoretical Experimental and Applied Physics: Series 8, Issue 1*, pages 1–9.

[Angerhofer, 1991] Angerhofer, A. (1991). 4.8 chlorophyll triplets and radical pairs. In Scheer, H., editor, *Chlorophylls*, pages 945–991. CRC Press.

[Austin and Erramilli, 1995] Austin, R. H. and Erramilli, S. (1995). Low-temperature spectroscopy. In *Biochemical Spectroscopy*, volume 246 of *Methods in Enzymology*, pages 131–168. Academic Press.

[Baniulis et al., 2008] Baniulis, D., Yamashita, E., Zhang, H., Hasan, S. S., and Cramer, W. A. (2008). Structure-function of the cytochrome b6f complex. *Photochemistry and Photobiology*, 84:1349–1358.

[Beeby et al., 1992] Beeby, A., Parker, A. W., Simpson, M. S., and Phillips, D. (1992). The effect of solvent deuteration on the photophysics of sulphonated aluminium phthalocyanine. *Journal of Photochemistry and Photobiology B: Biology*, 16(1):73–81.

[Berlin et al., 2006] Berlin, Y., Burin, A., Friedrich, J., and Köhler, J. (2006). Spectroscopy of proteins at low temperature. part i: Experiments with molecular ensembles. *Physics of Life Reviews 3*, pages 262–292.

[Berlin et al., 2007] Berlin, Y., Burin, A., Friedrich, J., and Köhler, J. (2007). Low temperature spectroscopy of proteins. part ii: Experiments with single protein complexes. *Physics of Life Reviews 4*, pages 64–89.

[Bruice, 2014] Bruice, P. Y. (2014). *Organic Chemistry, Seventh Edition*. Pearson Education Inc.

[Brunisholz and Zuber, 1992] Brunisholz, R. A. and Zuber, H. (1992). Structure, function and organization of antenna polypeptides and antenna complexes from the three families of rhodospirillaneae. *Journal of Photochemistry and Photobiology B: Biology, Issues 1-2*, 15:113–140.

[Bullough et al., 2009] Bullough, P. A., Qian, P., and Hunter, C. N. (2009). Reaction center-light-harvesting core complexes of purple bacteria. In Hunter, C. N., Daldal, F., Thurnauer, M. C., and Beatty, J. T., editors, *The Purple Phototrophic Bacteria*, volume 28 of *Advances in Photosynthesis and Respiration*, pages 155–179. Springer.

[Chen, 2008] Chen, P. (2008). Image of absorption spectra of chlorophylls, retrieved from http://bio1151b.nicerweb.net/locked/media/ch10/10_09photosynthwavelength.jpg (accessed may 4, 2021).

[Cogdell et al., 1997] Cogdell, R. J., Isaacs, N. W., Freer, A. A., Arrelano, J., Howard, T. D., Papiz, M. Z., Hawthornthwaite-Lawless, A. M., and Prince, S. (1997). The

structure and function of the lh2 (b800-850) complex from the purple photosynthetic bacterium rhodopseudomonas acidophila strain 10050. *Prog. Biophys. mole. Biol., No. 1*, 98:1–27.

[de Paula et al., 1995] de Paula, J. C., Robblee, J. H., and Pasternack, R. F. (1995). Aggregation of chlorophyll a probed by resonance light scattering spectroscopy. *Biophysical Journal*, 68:335–341.

[Du et al., 1998] Du, H., Fuh, R.-C. A., Li, J., Corkan, L. A., and Lindsey, L. A. (1998). Photochemcad: A computer-aided design and research tool in photochemistry. *Photochem. Photobiol.*, 68:141–142.

[Fidy et al., 1998] Fidy, J., Laberge, M., Kaposi, A., and Vanderkooi, J. (1998). Fluorescence line narrowing applied to the study of proteins. *Biochimica et Biophysica Acta (BBA) - Protein Structure and Molecular Enzymology*, 1386(2):331–351.

[Fraser et al., 1999] Fraser, N. J., Dominy, P. J., Ücker, B., Simonin, I., Scheer, H., and Cogdell, R. J. (1999). Selective release, removal, and reconstitution of bacteriochlorophyll a molecules into the b800 sites of lh2 complexes from rhodopseudomonas acidophila 10050. *Biochemistry*, 38:9684–9692.

[Frauenfelder et al., 1988] Frauenfelder, H., Parak, F., and Young, R. (1988). Conformational substates in proteins. *Annual Review of Biophysics and Biophysical Chemistry*, 17:451–479.

[Frauenfelder et al., 1991] Frauenfelder, H., Sligar, S. G., and Wolynes, P. G. (1991). The energy landscapes and motions of proteins. *Science, New Series, Issue 5038*, 254:1598–1603.

[Friedrich, 1995] Friedrich, J. (1995). [10] hole burning spectroscopy and physics of proteins. In *Biochemical Spectroscopy*, volume 246 of *Methods in Enzymology*, pages 226–259. Academic Press.

[Groot et al., 1995] Groot, M., Peterman, E., van Stokkum, I., Dekker, J., and van Grondelle, R. (1995). Triplet and fluorescing states of the cp47 antenna complex of photosystem ii studied as a function of temperature. *Biophysical Journal*, 68(1):281–290.

[Gupta, 2016] Gupta, V. (2016). *Principles and Applications of Quantum Chemistry*. Academic Press.

[Hasan et al., 2013] Hasan, S. S., Yamashita, E., Baniulis, D., and Cramer, W. A. (2013). Quinone-dependent proton transfer pathways in the photosynthetic cytochrome b6f complex. *Proc Natl Acad Sci USA.*, 110:4297–4302.

[Horton and Ruban, 2004] Horton, P. and Ruban, A. (2004). Molecular design of the photosystem ii light-harvesting antenna: photosynthesis and photoprotection. *Journal of Experimental Botany*, 56(411):365–373.

[Jankowiak et al., 2011] Jankowiak, R., Reppert, M., Zazubovich, V., Pieper, J., and Reinot, T. (2011). Site selective and single complex laser-based spectroscopies: A window on excited state electronic structure, excitation energy transfer, and electron–phonon coupling of selected photosynthetic complexes. *Chemical Reviews*, 111:4546–4598.

[Jankowiak et al., 2000] Jankowiak, R., Zazubovich, V., Rätsep, M., Matsuzaki, S., Alfonso, M., Picorel, R., Seibert, M., and Small, G. J. (2000). The cp43 core antenna complex of photosystem ii possesses two quasi-degenerate and weakly coupled qy-trap states. *J. Phys. Chem. B*, 104:11805–11815.

[Jones, 2009] Jones, M. (2009). Image of energy transfer in the purple bacterial photosystem, retrieved from http://photobiology.info/jones_files/jones-figure6.png (accessed april 11, 2021).

[Jones and Fleming, 2010] Jones, M. J. and Fleming, S. A. (2010). *Organic Chemistry, Fourth Edition*. W. W. Norton and Company.

[Kim et al., 1996] Kim, W. H., Reinot, T., Hayes, J. M., and Small, G. J. (1996). Nonphotochemical hole burning in hyperquenched glassy films of water: A pronounced deuteration effect. *The Journal of Chemical Physics*, 104:6415–6417.

[Klimov, 2003] Klimov, V. V. (2003). Discovery of pheophytin function in the photosynthetic energy conversion as the primary electron acceptor of photosystem ii. *Photosynthesis Research*, 76:247–253.

[Kosumi et al., 2018] Kosumi, D., Nishiguchi, T., Amao, Y., Cogdell, R. J., and Hashimoto, H. (2018). Singlet and triplet excited states dynamics of photosynthetic pigment chlorophyll a investigated by sub-nanosecond pump-probe spectroscopy. *J. Photochem. Photobiol. A: Chem*, 358:374–378.

[Krasnovsky, 1982] Krasnovsky, A. A. J. (1982). Delayed fluorescence and phosphorescence of plant pigments. *Photochem. Photobiol.*, 36:733–741.

[Kühlbrandt, 1995] Kühlbrandt, W. (1995). Structure and function of bacterial light-harvesting complexes. *Minireview*, 3:521–525.

[Law et al., 2004] Law, C. J., Roszak, A. W., Southall, J., Gardiner, A. T., Isaacs, N. W., and Cogdell, R. J. (2004). The structure and function of bacterial light-harvesting complexes. *Molecular Membrane Biology, Issue 3*, 21:183–191.

[Levenberg et al., 2017] Levenberg, A., Shafiei, G., Lujan, M. A., Giannacopoulos, S., Picorel, R., and Zazubovich, V. (2017). Probing energy landscapes of cytochrome b6f with spectral hole burning: Effects of deuterated solvent and detergent. *The Journal of Physical Chemistry B*, 121:9848–9858.

[Lyle et al., 1993] Lyle, P. A., Kolaczkowski, S. V., and Small, G. J. (1993). Photochemical hole-burned spectra of protonated and deuterated reaction centers of rhodobacter sphaeroides. *J. Phys. Chem.*, 97:6924–6933.

[Mauring et al., 1987] Mauring, K., Renge, I., Sarv, R., and Avarmaa, R. (1987). Fluorescence-detected triplet kinetics study of the specifically solvated chlorophyll a and protochlorophyll in frozen solutions. *Spectroschimica Acta No. 4*, 43A:507–514.

[Melkozernov and Blankenship, 2006] Melkozernov, A. N. and Blankenship, R. E. (2006). Photosynthetic functions of chlorophylls. In Grimm, B., Porra, R., Rüdiger, W., and

Scheer, H., editors, *Chlorophylls and Bacteriochlorophylls*, volume 25 of *Advances in Photosynthesis and Respiration*, pages 397–412. Springer, Dordrecht.

[Mukai et al., 1999] Mukai, K., Abe, S., and Sumi, H. (1999). Theory of rapid excitation-energy transfer from b800 to optically-forbidden exciton states of b850 in the antenna system lh2 of photosynthetic purple bacteria. *The Journal of Chemical Physics*, 103:6096–6102.

[Müller et al., 1998] Müller, J., Haarer, D., Khodykin, O. V., and Kharlamov, B. M. (1998). Investigation of spectral diffusion in pmma on timescales from 10-5 to 104 seconds via transient and photophysical hole burning. *Chem. Phys.*, 237:483–491.

[Najafi et al., 2012] Najafi, M., Herascu, N., Seibert, M., Picorel, R., Jankowiak, R., and Zazubovich, V. (2012). Spectral hole burning, recovery, and thermocycling in chlorophyll–protein complexes: Distributions of barriers on the protein energy landscape. *The Journal of Physical Chemistry B*, 116:11780–11790.

[Najafi et al., 2015] Najafi, M., Herascu, N., Shafiei, G., Picorel, R., and Zazubovich, V. (2015). Conformational changes in pigment-protein complexes at low temperatures - spectral memory and a possibility of cooperative effects. *The Journal of Physical Chemistry B*, 119:6930–6940.

[Nelson and Yocum, 2006] Nelson, N. and Yocum, C. F. (2006). Structure and function of photosystems i and ii. *Annu. Rev. Plant Biol.*, 57:521–565.

[Neupane et al., 2010] Neupane, B., Dang, N. C., Acharya, K., Reppert, M., Zazubovich, V., Picorel, R., Seibert, M., and Jankowiak, R. (2010). Insight into the electronic structure of the cp47 antenna protein complex of photosystem ii: hole burning and fluorescence study. *J. Am. Chem. Soc.*, 132:4214–4229.

[Neverov et al., 2015] Neverov, K. V., Jr, A. A. K., Zabelin, A. A., Shuvalov, V. A., and Shkuropatov, A. Y. (2015). Low-temperature (77 k) phosphorescence of triplet chlorophyll in isolated reaction centers of photosystem ii. *Photosynthesis research*, 125:43–49.

[Niedzwiedzki and Blankenship, 2010] Niedzwiedzki, D. M. and Blankenship, R. E. (2010). Singlet and triplet excited state properties of natural chlorophylls and bacteriochlorophylls. *Photosynth. Res.*, 106:227–238.

[Pirchi et al., 2011] Pirchi, M., Ziv, G., Riven, I., Cohen, S. S., Zohar, N., Barak, Y., and Haran, G. (2011). Single-molecule fluorescence spectroscopy maps the folding landscape of a large protein. *Nature Communications*, 2:1–7.

[Pittner et al., 2013] Pittner, S., Lehmann, D., Zahn, D. R. T., and Wagner, V. (2013). Charge transport analysis of poly(3-hexylthiophene) by electroreflectance spectroscopy. *Phys. Rev. B*, 87:115211.

[Ramanathan et al., 2013] Ramanathan, A., Savol, A., Burger, V., Chennubhotla, C. S., and Agarwal, P. K. (2013). Protein conformational populations and functionally relevant substates. *Accounts of Chemical Research, Issue 1*, 47:149–156.

[Rätsep et al., 2009] Rätsep, M., Linnanto, J., and Freiberg, A. (2009). Mirror symmetry and vibrational structure in optical spectra of chlorophyll a. *J. Chem. Phys.*, 130:194501.

[Rebane, 2008] Rebane, A. (2008). Image of variation of the homogeneous absorption spectrum with temperature, retrieved from https://physics.montana.edu/arebane/research/tutorials/hole_burning/images/shb_1-3.gif (accessed may 5, 2021).

[Reinot and Small, 2000] Reinot, T. and Small, G. J. (2000). Modeling of dispersive nonphotochemical hole growth kinetics data: Al-phthalocyanine tetrasulphonate in hyperquenched glassy water. *The Journal of Chemical Physics*, 113:10207–10214.

[Riesen and Hughes, 2003] Riesen, H. and Hughes, J. L. (2003). Massive enhancement of persistent spectral hole-burning in the r-lines of nangal(oxalate)3 · 9h2o/cr(iii) by partial deuteration. *Chemical Physics Letters*, 372:563–568.

[Riley et al., 2004] Riley, K., Jankowiak, R., Rätsep, M., Small, G. J., and Zazubovich, V. (2004). Evidence for highly dispersive primary charge separation kinetics and gross

heterogeneity in the isolated ps ii reaction center of green plants. *J. Phys. Chem. B*, 108:10346–10356.

[Ritz et al., 2002] Ritz, T., Damjanović, A., and Schulten, K. (2002). The quantum physics of photosynthesis. *ChemPhysChem*, 3:243–248.

[Robert et al., 2003] Robert, B., Cogdell, R. J., and van Grondelle, R. (2003). The light-harvesting system of purple bacteria. In Green, B. R. and Parson, W. W., editors, *Light-Harvesting Antennas in Photosynthesis*, volume 13 of *Advances in Photosynthesis and Respiration*, pages 169–194. Springer Science+Business Media Dorcrecht.

[Santabarbara et al., 2007] Santabarbara, S., Agostini, G., Casazza, A. P., Syme, C. D., Heathcote, P., Böhles, F., Evans, M. C., Jennings, R. C., and Carbonera, D. (2007). Chlorophyll triplet states associated with photosystem i and photosystem ii in thylakoids of the green alga chlamydomonas reinhardtii. *Biochimica et Biophysica Acta (BBA) - Bioenergetics*, 1767(1):88–105.

[Sapozhnikov, 1978] Sapozhnikov, M. N. (1978). Properties of the zero-phonon lines in the optical spectra of molecular crystals. *The Journal of Chemical Physics, 68(5)*, pages 2352–2361.

[Scheer, 2006] Scheer, H. (2006). An overview of chlorophylls and bacteriochlorophylls: Biochemistry, biophysics, functions, and applications. In Grimm, B., Porra, R., Rüdiger, W., and Scheer, H., editors, *Chlorophylls and Bacteriochlorophylls*, volume 25 of *Advances in Photosynthesis and Respiration*, pages 1–26. Springer, Dordrecht.

[Scholes and Fleming, 2000] Scholes, G. D. and Fleming, G. R. (2000). On the mechanism of light harvesting in photosynthetic purple bacteria: B800 to b850 energy transfer. *The Journal of Chemical Physics*, 104:1854–1868.

[Sebastien, 2010] Sebastien, A. (2010). Image of chloroplast's thylakoid membrane with different components, retrieved from https://en.citizendium.org/images/thumb/e/eb/thylakoid_membrane_gov.jpg/400px-thylakoid_membrane_gov.jpg (accessed may 4, 2021).

[Senge and Smith, 2004] Senge, M. O. and Smith, K. M. (2004). Biosynthesis and structures of the bacteriochlorophylls. In Blankenship, R. E., Madigan, M. T., and Bauer, C. E., editors, *Anoxygenic Photosynthetic Bacteria*, volume 2 of *Advances in Photosynthesis*, pages 137–151. Kluwer Academic Publishers.

[Shafiei et al., 2019] Shafiei, G., Levenberg, A., Lujan, M. A., Picorel, R., and Zazubovich, V. (2019). Evidence of simultaneous spectral hole burning involving two tiers of the protein energy landscape in cytochrome b_6f. *J. Phys. Chem. B*, 123:10930–10938.

[Shen, 2020] Shen, J.-R. (2020). Photosystem ii: Protein components, structure and electron transfer. In *Reference Module in Life Sciences*. Elsevier.

[Shooshtari, 2013] Shooshtari, S. M. N. (2013). *Modeling and Characterization of Protein Energy Landscape at Low Temperature using Spectral Hole Burning Spectroscopy*. PhD thesis, Concordia University.

[Sigma-Aldrich, 2021] Sigma-Aldrich (2021). National center for biotechnology information: Pubchem substance record for sid 24891877, sigma-aldrich, retrieved from https://pubchem.ncbi.nlm.nih.gov/substance/24891877 (accessed may 5, 2021).

[Suisalu et al., 1980] Suisalu, K. N. M. A. P., Avarmaa, R. A., and Krasnovsky, A. A. J. (1980). Phosphorescence of chlorophyll a and pheophytin a at liquid helium temperature. *Dokl. Akad. Nauk SSSR*, 251:729–731.

[Ter-Mikirtychev, 2017] Ter-Mikirtychev, V. (2017). Optical spectroscopy of rare-earth ions in the solid state. In Lindon, J. C., Tranter, G. E., and Koppenaal, D. W., editors, *Encyclopedia of Spectroscopy and Spectrometry (Third Edition)*, pages 481–491. Academic Press.

[Trempe et al., 2021] Trempe, A., Levenberg, A., Ortega, A. D. G., Lujan, M. A., Picorel, R., and Zazubovich, V. (2021). Effects of chlorophyll triplet states on the kinetics of spectral hole growth. *The Journal of Physical Chemistry B*, 125:3278–3285.

[Vries and Wiersma, 1980] Vries, H. D. and Wiersma, D. A. (1980). Photophysical and photochemical molecular hole burning theory. *J. Chem. Phys.*, 72:1851–1863.

[Wang et al., 2020] Wang, Y., Burgess, S. J., de Becker, E. M., and Long, S. P. (2020). Photosynthesis in the fleeting shadows: an overlooked opportunity for increasing crop productivity? issue 4. *The Plant Journal*, 101:874–884.

[Whitmarsh and Govindjee, 1999] Whitmarsh, J. and Govindjee (1999). Image of chemical structure of chlorophyll a molecule, retrieved from https://www.life.illinois.edu/govindjee/paper/fig4.gif (accessed may 4, 2021).

[Williams and Allen, 2009] Williams, J. C. and Allen, J. P. (2009). Directed modification of reaction centers from purple bacteria. In Hunter, C. N., Daldal, F., Thurnauer, M. C., and Beatty, J. T., editors, *The Purple Phototrophic Bacteria*, volume 28 of *Advances in Photosynthesis and Respiration*, pages 337–353. Springer, Dordrecht.

[Young and Beatty, 2003] Young, C. S. and Beatty, J. T. (2003). Multi-level regulation of purple bacterial light-harvesting complexes. In Green, B. R. and Parson, W. W., editors, *Light-Harvesting Antennas in Photosynthesis*, volume 13 of *Advances in Photosynthesis and Respiration*, pages 449–470. Springer Science+Business Media Dorcrecht.

[Zabelin et al., 2016] Zabelin, A. A., Neverov, K. V., Krasnovsky, A. A. J., Shkuropatova, V. A., Shuvalov, V. A., and Shkuropatov, A. Y. (2016). Characterization of the low-temperature triplet state of chlorophyll in photosystem ii core complexes: Application of phosphorescence measurements and fourier transform infrared spectroscopy. *Biochim Biophys Acta*, 1857:782–788.

[Zazubovich and Jankowiak, 2015] Zazubovich, V. and Jankowiak, R. (2015). Biophotonics of photosynthesis. In Andrews, D. L., editor, *Phototonics: Scientific Foundations, Technology and Applications, First Edition*, volume 4. John Wiley and Sons, Inc.

[Zazubovich et al., 2002] Zazubovich, V., Jankowiak, R., and Small, G. J. (2002). On b800 -> b800 energy transfer in the lh2 complex of purple bacteria. *Journal of Luminescence*, 98:123–129.